UNIVERSITY NAME (IN BLOCK CAPITALS)

Thesis Title

by

Author Name

A thesis submitted in partial fulfillment for the
degree of Doctor of Philosophy

in the

Faculty Name
Department or School Name

March 2018

Declaration of Authorship

I, AUTHOR NAME, declare that this thesis titled, 'THESIS TITLE' and the work presented in it are my own. I confirm that:

- This work was done wholly or mainly while in candidature for a research degree at this University.
- Where any part of this thesis has previously been submitted for a degree or any other qualification at this University or any other institution, this has been clearly stated.
- Where I have consulted the published work of others, this is always clearly attributed.
- Where I have quoted from the work of others, the source is always given. With the exception of such quotations, this thesis is entirely my own work.
- I have acknowledged all main sources of help.
- Where the thesis is based on work done by myself jointly with others, I have made clear exactly what was done by others and what I have contributed myself.

Signed: _____

Date: _____

"Write a funny quote here."

If the quote is taken from someone, their name goes here

UNIVERSITY NAME (IN BLOCK CAPITALS)

Abstract

Faculty Name
Department or School Name

Doctor of Philosophy

by Author Name

The Thesis Abstract is written here (and usually kept to just this page). The page is kept centered vertically so can expand into the blank space above the title too...

Acknowledgements

The acknowledgements and the people to thank go here, don't forget to include your project advisor...

Contents

List of Figures

List of Tables

Abbreviations

LAH **L**ist **A**bbreviations **H**ere

Physical Constants

Speed of Light $c = 2.997\ 924\ 58 \times 10^8\ \mathrm{ms}^{-\mathrm{S}}$ (exact)

Symbols

a	distance	m
P	power	W (Js^{-1})
ω	angular frequency	$rads^{-1}$

For/Dedicated to/To my...

Chapter 1

Theory

1.1 XY model and the BKT transition

The 2D XY model consists of a finite lattice of unit length spins that can rotate along the plane of the lattice. The Hamiltonian describing the system is given by

$$\mathcal{H} = -J \sum_{\langle i,j \rangle} \sum_{\{x,y\}} \boldsymbol{s}_{i,j} \cdot \boldsymbol{s}_{i+x,j+y} = -J \sum_{(i,j)} \sum_{\{x,y\}} \cos(\theta_{i,j} - \theta_{i+x,j+y})$$

where i, j signifies point (i, j) and $\{x, y\}$ are the pairs $\{0, 1\}\{0, 1\}$, i.e. nearest neighbours, and J is a constant. Periodic boundary conditions have been employed. We can form the continuum long wavelength (slowly varying) version of this equation by expanding in a Taylor series to obtain and keeping only terms to second order (as higher order terms will have Fourier transformed components greater than k^2 and we are ignoring those)

$$-J \sum_{(i,j)} \sum_{\{x,y\}} \left(1 - \frac{a^2}{2} \frac{(\theta_{i,j} - \theta_{i+x,j+y})^2}{a^2}\right).$$

The first term is a constant that can be ignored in what follows. Taking $a \to 0$, we have that $\sum_{(i,j)} a^2 \to \int \mathrm{d}x\, \mathrm{d}y$ and the terms in brackets become partial derivative, i.e. we obtain

$$\frac{J}{2} \int \mathrm{d}x\, \mathrm{d}y\, (\nabla\theta)^2$$

where now θ is a continuous variable. The Hamiltonian under consideration is invariant under global SO(2) transformation, i.e. in the replacement of $\theta \to \theta + \delta\theta$ as the change in cancelled in the cos terms. Because the system is two dimensional and interacting, it is impossible for the symmetry to be spontaneously broken, that is, the system cannot occupy a state in which all the spins point in the same direction. To demonstrate this,

we note that the probability of a configuration is given by

$$\mathcal{P}[\theta(\boldsymbol{r})] = \exp\left[-\beta J/2 \int \mathrm{d}^2\boldsymbol{r}\,(\nabla\theta)^2\right]$$

If we instead we decompose θ into its Fourier decomposition $\theta(\boldsymbol{r}) = \sum_{\boldsymbol{k}} \theta_{\boldsymbol{k}} e^{i\boldsymbol{k}\cdot\boldsymbol{r}}$ where the sum is over the Brillouin zone, we then obtain for the probability of $\theta(\boldsymbol{k})$

$$\mathcal{P}[\theta_{\boldsymbol{k}}] = \exp\left[-\beta J L^2/2k^2|\theta_{\boldsymbol{k}}|^2\right]$$

where L^2 denotes the system size and we use $\theta_{\boldsymbol{k}} = \theta^*_{-\boldsymbol{k}}$. Now $|\theta_{\boldsymbol{k}}|^2 = (\mathrm{Re}\,\theta_{\boldsymbol{k}})^2 + (\mathrm{Im}\,\theta_{\boldsymbol{k}})^2$ and we can write the probability of a configuration as

$$\begin{aligned}\mathcal{P}[\{\theta_{\boldsymbol{k}}\}] &= \prod_{\boldsymbol{k}} \exp\left[-\beta J L^2/2k^2|\theta_{\boldsymbol{k}}|^2\right] \\ &= \prod_{\boldsymbol{k},k_x>0} \exp\left[-2\beta J L^2/2k^2((\mathrm{Re}\,\theta_{\boldsymbol{k}})^2 + (\mathrm{Im}\,\theta_{\boldsymbol{k}})^2)\right]\end{aligned}$$

where in the second we restrict ourselves to the positive x and thus obtain completely decoupled Gaussian variables with variance $1/\beta J L^2$. Then the variances of $\theta_{\boldsymbol{k}}$ are given by

$$\langle\theta_{\boldsymbol{k}}\theta_{\boldsymbol{k}'}\rangle = \langle\mathrm{Re}\,\theta_{\boldsymbol{k}}\,\mathrm{Re}\,\theta_{\boldsymbol{k}'}\rangle + \langle\mathrm{Im}\,\theta_{\boldsymbol{k}}\,\mathrm{Im}\,\theta_{\boldsymbol{k}'}\rangle = \delta_{\boldsymbol{k},-\boldsymbol{k}'}/\beta J L^2$$

Now to calculate the average magnetisation we require to know

$$\left\langle\theta(\boldsymbol{r})\theta(\boldsymbol{r}')\right\rangle = \sum_{\boldsymbol{k},\boldsymbol{k}'} e^{i\boldsymbol{k}\cdot\boldsymbol{r}+i\boldsymbol{k}'\cdot\boldsymbol{r}'}\,\langle\theta_{\boldsymbol{k}}\theta_{\boldsymbol{k}'}\rangle = \frac{1}{\beta J L^2}\sum_{\boldsymbol{k}}\frac{e^{i\boldsymbol{k}\cdot(\boldsymbol{r}-\boldsymbol{r}')}}{k^2}$$

which can be replaced by an integral by $1/L^2\sum_{\boldsymbol{k}} \to \int \mathrm{d}^2\boldsymbol{k}\,/(2\pi)^2$ so that we obtain

$$\frac{1}{\beta J}\int\frac{\mathrm{d}^2\boldsymbol{k}}{(2\pi)^2}\frac{e^{i\boldsymbol{k}\cdot(\boldsymbol{r}-\boldsymbol{r}')}}{k^2}$$

The negative of the integral is the Green's function of ∇^2:

$$-\int\frac{\mathrm{d}^2\boldsymbol{k}}{(2\pi)^2}\nabla^2\frac{e^{i\boldsymbol{k}.(\boldsymbol{r}-\boldsymbol{r}')}}{k^2} = \int\frac{\mathrm{d}^2\boldsymbol{k}}{(2\pi)^2}k^2\frac{e^{i\boldsymbol{k}.(\boldsymbol{r}-\boldsymbol{r}')}}{k^2} = \delta^2(\boldsymbol{r}-\boldsymbol{r}')$$

Assuming a solution V that depends only on $|\boldsymbol{r}|$, which we expect for a mean in the XY model, we can find a solution with the divergence thoerem:

$$\int\nabla\cdot\nabla V\,\mathrm{d}^2\boldsymbol{r}\int r\nabla V\,\mathrm{d}\Omega = 2\pi r\nabla V = 1.$$

With $\nabla V = \partial V/\partial r$ this is $V(r) = \ln(r/a)/2\pi$ where the constant a is of the order of the lattice spacing. Finally, we need to use

$$\left\langle e^{A}\right\rangle = e^{\left(\langle A\rangle + \frac{1}{2}\langle A^2\rangle\right)}$$

for any linear combination A of Gaussian distributed variables. The mean value of the magnetisation is given by

$$\langle \cos\theta(\boldsymbol{r})\rangle = \mathrm{Re}\left\langle e^{i\theta(\boldsymbol{r})}\right\rangle = \mathrm{Re}\, e^{\left(i\langle\theta(\boldsymbol{r})\rangle - \frac{1}{2}\langle\theta(\boldsymbol{r})^2\rangle\right)}$$

Now $\langle\theta(\boldsymbol{r})\rangle = 0$ as it is the sum of the Gaussian distributed variables. The second term in the exponential, as we have just found, is $\frac{1}{2}\log(0)$. We thus have

$$\langle \cos\theta(\boldsymbol{r})\rangle = 0$$

and have therefore shown there is no spontaneous symmetry breaking. For free, we can calculate the spin correlations in space $\langle \cos\theta(\boldsymbol{r}-\boldsymbol{r}')\rangle$. Using the same method as before, the term in the exponential $\left\langle(\theta(\boldsymbol{r})-\theta(\boldsymbol{r}'))^2\right\rangle =$

$$2\left\langle\theta(\boldsymbol{r})^2\right\rangle - 2\left\langle\theta(\boldsymbol{r})\theta(\boldsymbol{r}')\right\rangle = \frac{\log(|\boldsymbol{r}-\boldsymbol{r}'|/a)}{\beta J\pi}$$

Thus, the correlations in space are of the form

$$\left\langle \cos\theta(\boldsymbol{r}-\boldsymbol{r}')\right\rangle \propto \frac{1}{|\boldsymbol{r}-\boldsymbol{r}'|^{\eta}}$$

for an exponent η. We then see that while there is no spontaneous symmetry breaking, there still exists a phase with 'algebraic' decay of correlations. Since in making the continuum assumption we only retained the leading order term in the Taylor expansion, we are implicitly assuming assuming large J that penalises large fluctuations of the spins. This is the low temperature phase. Assuming J small, we may expand the exponential of the original Hamiltonian in powers of J so that the partition function approximately:

$$\mathcal{Z} = \int \prod_{\boldsymbol{r}} \mathrm{d}\theta(\boldsymbol{r}) \prod_{\boldsymbol{r}'} [1 + \beta J\cos\big(\theta(\boldsymbol{r}) - \theta_(\boldsymbol{r}')\big) + \mathcal{O}(J^2)]$$

In determining the correlations in this regime, we note that any integral of the form

$$\int_0^{2\pi} \mathrm{d}\theta_k \cos(\theta_i - \theta_j)$$

is zero whereas

$$\int_0^{2\pi} \mathrm{d}\theta_k \cos(\theta_i - \theta_j)\cos(\theta_j - \theta_k) = \pi \cos(\theta_i - \theta_k)$$

Thus for the correlation we have

$$\langle \cos(\theta(\boldsymbol{r}) - \theta(\mathbf{0}))\rangle \propto (\pi J)^{|\boldsymbol{r}|}$$

as there an order $|\boldsymbol{r}|$ of cosine terms in the product that are required to 'connect' $\mathbf{0}$ to $\boldsymbol{r}$. We may rewrite this expression as $\exp[-|\boldsymbol{r}|/\xi]$ where $\xi^{-1} = 1/\pi J$ and is the 'correlation length' of the system. It quantifies the distance that the spins are correlated. This intuitive approach has revealed that the, in high temperature phase, correlations decay exponentially. The two types of decay – algebraic and exponential – are hallmarks of two phases in 2D systems, and the transition between the two is known as the BKT transition. More rigorous analysis reveals that the correlation length diverges at the critical point of the transition, and tends to zero as one moves away in either direction.

What differentiates the two phases? The essential insight is that the system enables the existence of topoligcal defects known as 'vortices'. This means that we cannot continuously deform a state with vortices into one without them, and thus it cannot be obtained through perturbation theory. To see their origin, note that the phase at each point is restricted to $[0, 2\pi]$, i.e. it is compact, and so the circulation, defined by

$$\int \nabla\theta \cdot \mathrm{d}\boldsymbol{l} = 2\pi n$$

must be restricted to $2\pi n$ where n is an integer so that the phase angle is not multiple valued. Now by the gradient theorem we know that if the gradient is everywhere defined inside the loop then this loop integral should be zero, already signaling that there must be a singularity for vortices to exist. Phase transitions are manifested by singularities in various quantities, and it is indeed it is in the absence or presence of vortices that is indicative of the phase the system occupies.

To obtain a better intuition for the subject, let us consider an isotropic solution $\nabla\theta = \frac{n}{r}\hat{\boldsymbol{r}}$. The integer n is known as the charge of the vortex, as then the solution is $\theta(\boldsymbol{r}) = \log(r)$ which describes a Coulombic charge in two dimensions. This provides a revealing picture for the system: in the low temperature phase the 'charges' are bound, but increasing the temperature beyond the transition is marked by an unbinding and proliferation of these vortices. Since the free energy $F = U - TS$ is minimised at a given temperature and volume, the proliferation at the critical point must mean the entropy increase is more favourable than the energy increase.

To estimate both, imagine that we have one vortex in the system. We use our expression for the energy

$$\int \mathrm{d}^2\boldsymbol{r}\,|\nabla\theta|^2 \propto \log(L)$$

where L is the system size. The number of places to put the vortex is proportional to L^2, so the entropy $k\log\Omega$ must also be proportional to $\log L$. As both have this proportionality, it is then clear that, at the critical point, $U - T_c S$ makes vortex proliferation favourable. All these points will come into play in a modified form in the study of polariton condensates.

After considering equilibrium issues, what of dynamics? We describe [**2016PhRvB..94j4521S**] the evolution of $\theta_{i,j}$ according the Langevin equation

$$\partial_t\theta_{i,j} = -\Gamma\frac{\delta\mathcal{H}}{\delta\theta_{i,j}} + \eta = -\Gamma\frac{\partial\mathcal{H}}{\partial\theta_{i,j}} + \eta$$

where η is a Guassian white noise term $\langle\eta(\boldsymbol{r},t),\eta(\boldsymbol{r}',t')\rangle = 2\Delta\delta(t-t')\delta(\boldsymbol{r}-\boldsymbol{r}')$. In the discrete version this is

$$\partial_t\theta_{i,j} = +\Gamma J\sum_{\{x,y\}}\sin(\theta_{i,j} - \theta_{i+x,j+y})$$

where $\{x,y\}$ are as before. The continuum version of this equation requires $\delta\mathcal{H}/\delta\theta$ which is

$$\frac{\delta\mathcal{H}}{\delta\theta} = \frac{J}{2}\int \mathrm{d}^2\boldsymbol{r}\,2(\nabla\theta)(\nabla\delta\theta).$$

Intgerating by parts we find that the integrand is zero for $J\nabla^2\theta$ so the equation is

$$\partial_t\theta = -\Gamma J\nabla^2\theta + \eta.$$

We will see that this is the equation of our equation describing the long wavelength behaviour of the condensate phase when we are in a certain regime.

1.2 XY model scaling violations

To understand the approach taken in the project, we describe the approach taken in [1] to determine dynamical evolution of the correlation length ξ as the system XY system is quenched from the disordered (high temperature) phase to the ordered (low temperature) phase. Using renormalisation group methods [**Janssen1989**], the dynamical exponent z is predicted to be 2 so that the correlation length grows as $\xi(t) = t^{1/2}$. To test this prediction, for various system sizes a plot of the time dependent Binder cumulant defined

by

$$g_L(t) = 2 - \frac{\left\langle \boldsymbol{M}^2 \right\rangle^2}{\left\langle \boldsymbol{M}^4 \right\rangle}$$

was plotted where $\boldsymbol{M}(t)$ is the magnetisation (the average of $(\cos\theta_{i,j}, \sin\theta_{i,j})$ on the lattice. The mean of $\boldsymbol{M}$ is over independent Monte Carlo runs. In a disordered condition where each spin is random, each component magnetisation is the sum of independent uniformly distributed numbers, and so by the central limit theorem are approximately Gaussian distributed. Then $\left\langle \boldsymbol{M}^2 \right\rangle^2 / \left\langle \boldsymbol{M}^4 \right\rangle$ is 2, so g_L is 0. In an ordered state where all spins are aligned, the ratio is one, and g_L is 1. The Binder cumulant is thus a convenient quantity to act as an ordered parameter.

Crucially, it is dimensionless. Therefore, for different system sizes, plotting the Binder cumulant as a function of another dimensionless quantity should result in all the curves 'collapsing' into one. Since we are varying the system size L, the ratio $\xi^2/L^2 = t/L^2$ is appropriate.

This was done in two cases: first in the quench from a completely ordered phase to one below the critical temperature, where $z = 2$ provided a good collapse. In the quench from the random initial condition to the ordered phase, however, a much higher exponent $z = 2.35$ was required to achieve the same quality in collapse. The disparity was explained by the requirement of vortex-antivortex binding necessary when queching from the disordered initial condition, which slows the approach to equilibrium. Indeed, a modification of the functional form of ξ was found to be necessary, and was $\xi(t) = (t/\log(t/t_0))^{1/2}$.

The physical origin of this was in the friction and attracted experienced by the vortices. For the attraction, we determined earlier that the vortices behave as 2D Coulombic charges, and thus the force between them is proportional to $1/R$ where R is the vortex distance. The friction was determined from the evolution equation (without noise, or $T = 0$), i.e. $\partial_\theta = -\delta H/\delta\theta$ (the prefactors being set to 1). If $\theta(x, y, t) = \theta_v(x - vt, y)$ is the vortex motion is now

$$\frac{\mathrm{d}E}{\mathrm{d}t} = \int \mathrm{d}^2\boldsymbol{r}\, \frac{\delta E}{\delta\theta}\frac{\partial\theta}{\partial t} = -\int \mathrm{d}^2\boldsymbol{r} \left(\frac{\partial\theta}{\partial t}\right)^2 = -v^2 \int \mathrm{d}^2\boldsymbol{r} \left(\frac{\partial\theta_v}{\partial x}\right)^2$$

Now for a frictional force $-\gamma\dot{x}$ we see that the last integral must be the friction constant. Using the equilibrium vortex configuration we found earlier, which is isotropic, and hence we replace the derivative by x with the gradient, we see that the zero velocity vortex friction is the equilibrium energy, and thus scales like $\log R$, the vortex distance.

Taking the correlation length as the vortex distance, the velocity of the vortices is $\frac{\mathrm{d}\xi}{\mathrm{d}t} \sim F/\gamma \sim 1/(\xi\log\xi)$ so that $\xi \sim (t/\log t)^{1/2}$.

1.3 Mapping to the KPZ Equation

We now in what way our polariton condensate relates to the XY model. Previously we discussed two pumping regimes for the microcavity: incoherent and the OPO regimes. The long wavelength dynamics of the phase in both cases is governed by the compact anisotropic KPZ equation

$$\partial_t\theta = D_x\frac{\partial^2\theta}{\partial x^2} + D_y\frac{\partial^2\theta}{\partial y^2} + \lambda_x\left(\frac{\partial\theta}{\partial x}\right)^2 + \lambda_y\left(\frac{\partial\theta}{\partial y}\right)^2 + \eta$$

where η is the Gaussian white noise term as before. We see that if the λs are set to zero (the Ds can always be set to one by rescaling the coordinates) we reobtain the equation for the XY model evolution.

However, the physical origin and the interpretation of θ is different in both cases, which will be discussed. First, as we described earlier polariton system can form a condensate by adjusting the drive parameters appropriately, and hence we can describe the condensate by a macroscopic wave function $\rho(\boldsymbol{r})e^{i\theta(\boldsymbol{r})}$. Since the phase angle is compact, by the same arguments as before, vortices are allowed to exist.

In the incoherent pump regime the dynamics of the condensate can be phenomenologically described by the dissipative Gross-Pitaevskii equation

$$\partial_t\psi(\boldsymbol{r},t) = -\frac{\delta H_d}{\delta\psi^*} + i\frac{\delta H_c}{\delta\psi^*} + \eta$$

where H_d and H_c are responsible for the coherent and dissipative dynamics and are given by

$$H_l = \int r_l|\psi|^2 + K_l^x|\partial_x\psi|^2 + K_l^y|\partial_y\psi|^2 + \tfrac{1}{2}u_l|\psi|^4$$

where $l = \{c, d\}$. The last term is a complex Gaussian white noise. The equation then reads

$$\partial_t\psi = -r_{\text{eff}}\psi + K^x_{\text{eff}}\partial_x^2\psi + K^y_{\text{eff}}\partial_y^2\psi - u_{\text{eff}}|\psi|^2\psi + \eta$$

where $A_{\text{eff}} = A_d - iA_c$. To simplify this equation, and in particular to determine an equation only dependent on θ, the condensate is expanded about a mean $(M_0 + \chi)e^{i\theta}$ where M_0 is set to be a static and uniform solution when $\eta = 0$ and $\theta = 0$. This gives $r_{\text{eff}}M_0 = -u_{\text{eff}}M_0^3$. The coeffient r_c is arbitrary and can be set by a local and time dependent transformation $\psi' = \psi e^{i\omega t}$, and this freedom is used to set $r_c = -u_cM_0^2$ and $r_d = -u_dM_0^2$. The physical origin of the other terms is as follows: r_d is the particle loss rate less the pump rate. Clearly the loss rate depends on the density of polaritons, and in the incoherent regimes a sufficient density is required for polariton creation. The K_c terms are the momentum coefficents in the x and y directions, inversely proportional

to m_x and m_y, while K_d are diffusion-like terms. Finally, the u_c term describes a two polariton interaction, and u_d is also a loss term but is non linear. The latter ensures that the polariton density does not grow without bound.

Substituting the mean expansion and linearising the χ fluctuation (also ignoring terms like $\partial_x\chi\partial_x\theta$), gives

$$\partial_t\chi = -2u_dM_0^2\chi - K_c^xM_0\partial_x^2\theta - K_c^yM_0\partial_y^2\theta - K_d^xM_0(\partial_x\theta)^2 - K_d^yM_0(\partial_y\theta)^2 + \mathrm{Re}\,\eta$$

$$M_0\partial_t\theta = -2u_cM_0^2\chi + K_d^xM_0\partial_x^2\theta + K_d^yM_0\partial_y^2\theta - K_c^xM_0(\partial_x\theta)^2 - K_c^yM_0(\partial_y\theta)^2 + \mathrm{Im}\,\eta$$

where the real and imaginary parts were equated. In the low frequency limit, the left hand side is negligible compared to the first term on the right as as it has a time derivative, therefore can be ignored. The first equation can be then be solved for χ and substituted into the second, from which the KPZ equation is obtained. That the long wavelength limit results in only θ dependence is as expected as the U(1) symmetry (clear from the Hamiltonian) means that the excitation about small k is 'gapless' in that the energy of the excitation tends to zero (since a slowly varying rotation in space can be made to require arbitrarily small energy). In contrast, excitations of the other variables are 'gapped' and the dispersion does not tend to zero at low k but some finite value as there is no corresponding symmetry. Thus we need only retain θ dependence.

For the coherent pump regime, purportedly the same dynamics is followed. However, here an ab initio rather than phenomlogical model is possible, and the meaning of θ is different: $\theta = \theta_s - \theta_i$ where s and i stand for the signal and idler modes. There again exists a U(1) symmetry as now polariton scattering is described by terms such as $\psi_s\psi_i\psi_p^{*2}$+h.c. which are invariant under a transformation $\psi_s \to \psi_s e^{i\alpha}$, $\psi_i \to \psi_i e^{-i\alpha}$, and ψ_p kept the same. This symmetry results in a gapless excitation and the KPZ equation is obtained with the modified θ.

To obtain the discretised version of this equation, the linear terms are transformed as before in the XY model, i.e. by

$$\partial_x^2\theta_{i,j} = -\sum_{x=\{-1,1\}} \sin(\theta_{i,j} - \theta_{i+x,j})$$

and analogously for the y direction. The nonlinear terms are the second order coefficients in the expansion of cos, so the prescription for these is

$$(\partial_x\theta_{i,j})^2 = -\sum_{x=\{-1,1\}} (\cos(\theta_{i,j} - \theta_{i+x,j}) - 1)$$

and analogously for the y direction. There is no factor of 2 as we are summing two such cos terms in each case.

1.4 Polariton Condensate Regimes

Using the KPZ equation parameters, the regimes of the condensate are parametrised by the scaled nonlinearity

$$g \equiv \lambda_x^2 / D_x^2 \sqrt{D_x D_y}$$

and the scaled anistropy

$$\Gamma = \lambda_y D_x / \lambda_x D_y.$$

For the KPZ equation to be stable, the Ds must be positive. The sign of the anistropy therefore depends on the signs of the λs, and their relative sign matters.. The cases $\Gamma > 0$ and $\Gamma < 0$ are called the weak and strong anistropy phases, respectively.

To determine the long range behaviour in the absense of vortices, rernormalisation group (RG) analysis has been peformed. The essential idea is as follows: over small length scale the system is course grained so is in a sense averaged. A microscropic length scale of the system (such as lattice spacing) is then obtained by shrinking the course grained length scale down to the lattice spacing. This process results in a new description of the system with the parameters adjusted. After repeated application of this procedure, a 'flow' of the parameter values is obtained (essentially a phase portrait) and the terms that are non zero at the fixed points, which correspond to points where the correlation length is zero, it shrinking after each iteration, are the terms that are important. Two cases are important. For the weak anisotropic regime all flow lines tend to $g = \inf$ and $\Gamma = 1$. In the strongly anisotropic regime there is a fixed point at $g = 0$ and $\Gamma = -1$. This is the XY model regime where $\lambda = 0$ and one expects BKT physics.

In practice, only the weakly anisotropic regime is accesible in the case of incoherent pumping, whereas for the OPO pumping it is experimentally viable to traverse different regimes by the adjustment of the pump strength. We shall now describe the various possible

Chapter 2

Method

2.1 Data Generation

The evolution of the condensate phase was simulated using code written in C++. This defined the codensate as a square lattice consisting of N^2 points, where N is the linear size of the lattice, and each point restricted to be between $[0, 2\pi]$. Initially, the angle of each point was random, the system therefore being in the disordered phase. The simulation updated each lattice point according to the compactified and discretised equation:

$$\begin{aligned}\theta_{i,j}(t+\mathrm{d}t) = \theta_{i,j}(t) + \mathrm{d}t\,[&- D_x(\cos(\theta_{i,j}-\theta_{i+1,j}) + \cos(\theta_{i,j}-\theta_{i-1,j}) - 2) \\ &- D_y(\cos(\theta_{i,j}-\theta_{i,j-1}) + \cos(\theta_{i,j}-\theta_{i,j+1}) - 2) \\ &- \frac{\lambda_x}{2}(\sin(\theta_{i,j}-\theta_{i+1,j}) + \sin(\theta_{i,j}-\theta_{i-1,j})) \\ &- \frac{\lambda_y}{2}(\sin(\theta_{i,j}-\theta_{i,j-1}) + \sin(\theta_{i,j}-\theta_{i,j+1}))] \\ &+ 2\pi c_L \times \sqrt{\mathrm{d}t} \times \xi\end{aligned}$$

where $\theta_{i,j}(t)$ is the value of the condensate at points i, j of the lattice and $\mathrm{d}t$ is the timestep used. Periodic boundary conditions were used. The final term is the stochastic term where ξ is a uniformaly distributed random number (restricted to $[-0.5, 0.5]$) that was also added at each timestep. Finally, for all simulations D_x and D_y were set to 1 as the coordinates can always be rescaled to ensure this.

The timestep was initially chosen to be $\mathrm{d}t = 0.01$ and this was the value used to generate the significant data. However, other values were considered with: namely, $\mathrm{d}t = 0.02$ and $\mathrm{d}t = 0.001$ with system size 32. Figure. **??** comes the Binder cumulant for this system size for the three values of $\mathrm{d}t$. The evolution for $\mathrm{d}t = 0.02$ did not follow that of $\mathrm{d}t = 0.01$,

implying that $\mathrm{d}t = 0.02$ was potentially too large of a timestep, whereas the behaviour of $\mathrm{d}t = 0.01$ reasonably matched that of $\mathrm{d}t = 0.001$, demonstrating that $\mathrm{d}t = 0.01$ was an appropriate timestep for the simulation, and a smaller one was computationally unnecessary.

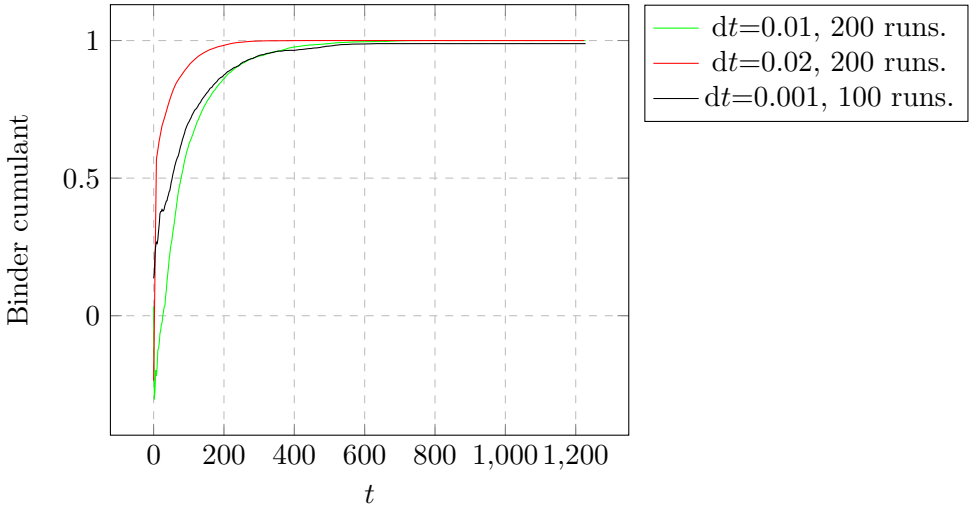

FIGURE 2.1: The Binder cumulant convergence for $L = 32$ at different values of $\mathrm{d}t$. The convergence of $\mathrm{d}t = 0.001$ compared to $\mathrm{d}t = 0.01$ suggests that a timestep of $\mathrm{d}t = 0.001$ was unnecessary, while the behaviour of $\mathrm{d}t = 0.02$ although qualitatively correct, deviated from that $\mathrm{d}t = 0.02$ significantly to be considered trustworthy.

The value of c_L at which the phase transition occurs was determined. Figure. **??** shows the number of vortices $t = 400$ for a system size of 64 at various values of c_L. The value $c_L = 0.2$ was then chosen for the remainder of project. For the value of $c_L = 0.1$ the Binder cumulant did not approach one at all in the case of $L = 128$, as shown in Figure. **??**. This is likely a numerical artefact and can be explained by the existence of vortices stuck to lattice sites and not able to anihilate due to the low noise. The number of vortices is higher in Figure. **??** for $c_L = 0.1$ than higher values below the transition. XX shows a snapshat of the system for one realisation to illustrate this. This issue was also mentioned in XX.

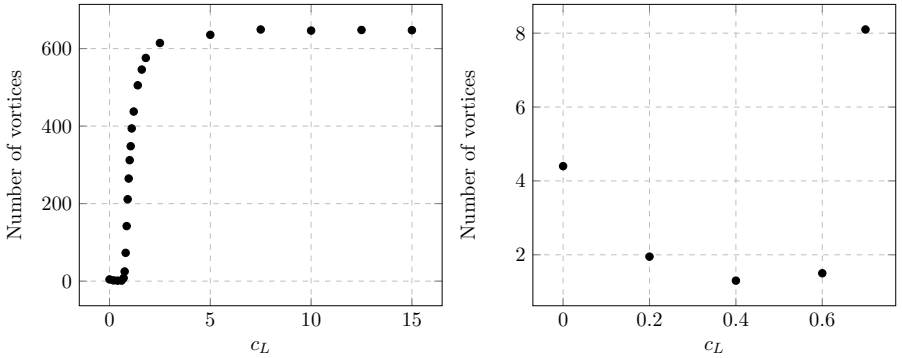

FIGURE 2.2: The number of vortices at the end of a simulation ($t = 400$) as a function of c_L for $L = 64$ with 20 runs.

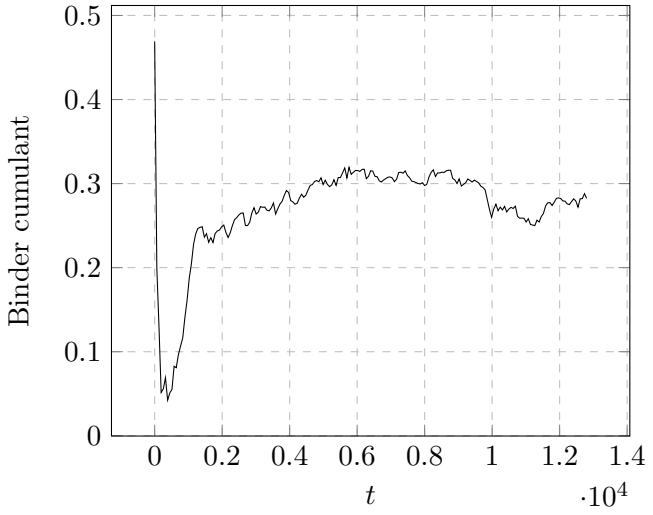

FIGURE 2.3: The Binder cumulant for $L = 128$ and $c_L = 0.1$. Despite being in the ordered phase, the Binder cumulant does not converge to near one due to the vortices.

2.2 Data Extraction

Using the generated data, the Binder cumulant was calculated as follows: for each timestep of a simulation, the magnetisation $\boldsymbol{M}$, defined by

$$\boldsymbol{M} = \frac{1}{N^2}\sum_{i,j}(\cos(\theta_{i,j}), \sin(\theta_{i,j})),$$

where the sum is over all lattice points, was calculated. The averages (over all the realisations) $\left\langle \boldsymbol{M}^2 \right\rangle$ and $\left\langle \left(\boldsymbol{M}^2\right)^2 \right\rangle$ were then used in the Binder cumulant given by

$$g = 2 - \frac{\left\langle (\boldsymbol{M}^2)^2 \right\rangle}{\left\langle \boldsymbol{M}^2 \right\rangle^2}$$

To estimate the error, the Binder cumulant was considered to be a function of the variables $\boldsymbol{M}^2 >$, i.e.

$$g = 2 - N\frac{\sum_i (\boldsymbol{M}_i^2)^2}{\left(\sum_i \boldsymbol{M}_i^2\right)^2}$$

where the sum is over every realisation and N is the number of realisations. These variables are indentical and independent, so the error of each is the same and is approximated by

$$\sigma^2_{\boldsymbol{M}^2} = \frac{1}{N-1}\sum_i (\boldsymbol{M}_i^2 - \left\langle \boldsymbol{M}^2 \right\rangle)^2 = \frac{N}{N-1}(\left\langle (\boldsymbol{M}^2)^2 \right\rangle - \left\langle \boldsymbol{M}^2 \right\rangle^2).$$

Using error propagation, the error on the Binder cumulant is

$$\begin{aligned}
\sigma_g^2 &= 4N^2 \sum_k \left(-\frac{\boldsymbol{M}_k^2}{\left(\sum_i \boldsymbol{M}_i^2\right)^2} + \frac{\sum_i (\boldsymbol{M}_i^2)^2}{\left(\sum_i \boldsymbol{M}_i^2\right)^3} \right)^2 \sigma_{\boldsymbol{M}^2} \\
&= \frac{4N^3}{N-1} \left(\left\langle (\boldsymbol{M}^2)^2 \right\rangle - \left\langle \boldsymbol{M}^2 \right\rangle^2 \right) \sum_k \left(\frac{(\boldsymbol{M}_k^2)^2}{\left(\sum_i \boldsymbol{M}_i^2\right)^4} + -2\frac{\boldsymbol{M}_k^2 \sum_i (\boldsymbol{M}_i^2)^2}{\left(\sum_i \boldsymbol{M}_i^2\right)^5} + \frac{\left(\sum_i (\boldsymbol{M}_i^2)^2\right)^2}{\left(\sum_i \boldsymbol{M}_i^2\right)^6} \right) \\
&= \frac{4N^3}{N-1} \left(\left\langle (\boldsymbol{M}^2)^2 \right\rangle - \left\langle \boldsymbol{M}^2 \right\rangle^2 \right) \left(\frac{N \left\langle (\boldsymbol{M}^2)^2 \right\rangle}{N^4 \left\langle \boldsymbol{M}^2 \right\rangle^4} - 2\frac{N^2 \left\langle \boldsymbol{M}^2 \right\rangle \left\langle (\boldsymbol{M}^2)^2 \right\rangle}{N^5 \left\langle \boldsymbol{M}^2 \right\rangle^5} + \frac{N^3 \left\langle (\boldsymbol{M}^2)^2 \right\rangle^2}{N^6 \left\langle \boldsymbol{M}^2 \right\rangle^6} \right) \\
&= \frac{4}{N-1} \left(\left\langle (\boldsymbol{M}^2)^2 \right\rangle - \left\langle \boldsymbol{M}^2 \right\rangle^2 \right)^2 \frac{\left\langle (\boldsymbol{M}^2)^2 \right\rangle}{\left\langle \boldsymbol{M}^2 \right\rangle^6}
\end{aligned}$$

which is proporiotnal to $1/N$, as expected.

To calculate the number of vortices or anti-vortices, we use a discretised version of their defining equation. The 'loop', starting at a point $\theta_{i,j}$, is the path

$$\theta_{i,j} \to \theta_{i+1,j} \to \theta_{i+1,j+1} \to \theta_{i,j+1} \to \theta_{i,j}$$

and the value of one angle minus the value of the previous angle is calculated and all such differences are summed. If the total is greater than or equal to 2π, there is a vortex, whereas if the total is less than or equal to -2π, there is an antivortex.

Chapter 3

Results

Simulations were peformed on system sizes $L = 40, 48, 64, 80, 104, 128$ with the λs taken from zero to one in steps of 0.2 and also 1.5 where λ_x and λ_y had the same magnitude and the same or opposite signs.

3.1 Linear Case

Figure. **??** overlays the Binder cumulant evolution for different sizes in the linear ($\lambda_x = \lambda_y = 0$) case which corresponds to the XY model. Figure. **??** does the same but plotted with respect to $t/L^2 \log t$ where the collapse is expected. As is clear, this reobtains the result from [1] while using Stochastic evolution rather than Monte Carlo and provides confidence in the results for the non-linear cases. The collapse is not perfect: Figures **??** and **??**, which display the Binder cumulant as a function of the number of realisations for all the system sizes, show how far apart the curves are. A value of $t/L^2 \log t$ was calculated for $L = 40$ for two points in the simulation, namely, midway through and three quarters of the way thourgh, and the corresponding t was chosen for all other system sizes that was closest to this value. In this report we call these the midway and three quarters graph for brevity. For the first case, the uncertainties of the points do not all cross, although none are isolated. In the second case, the collapse is weaker and $L = 48$ is consistently isolated, as can be seen from the graph of the collapse. This also occurs for $L = 64$ earlier on in the simulation. For $L = 48$ there could be an underestimation of the error, and there is a slight downward decrease in its value as the number of realisations is increased. Ideally one would perform further simulations to ensure this, but this was not possible in the time constraints of the project.

With those caveats in mind, we may be assured that the result has been obtained, and this is further corroborated by the plots of $\log n_v$, where n_v is the number of vortices, as

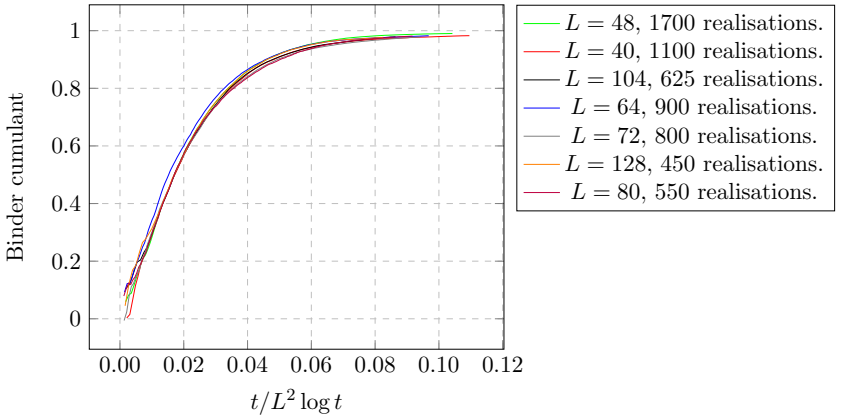

FIGURE 3.1: The Binder cumulant as a function of $t/L^2 \log t$ for different sizes with $\lambda_x = \lambda_y = 0$.

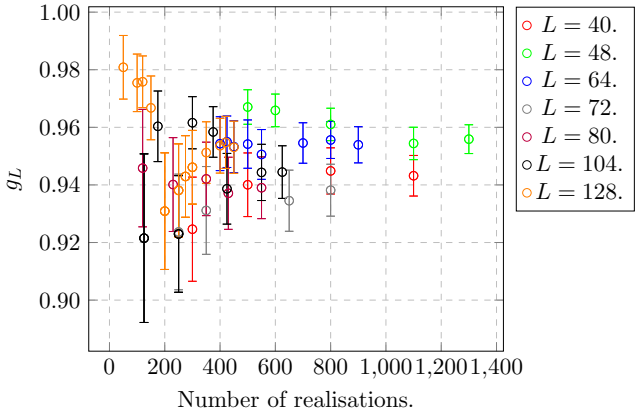

FIGURE 3.2: The uncertainty in the Binder cumulant as a function of the number of realisations at a point closest to $t/L^2 \log t$ for $t = 6500$ (the mid-point of the simulation) for $L = 40.\lambda_x = \lambda_y = 0$.

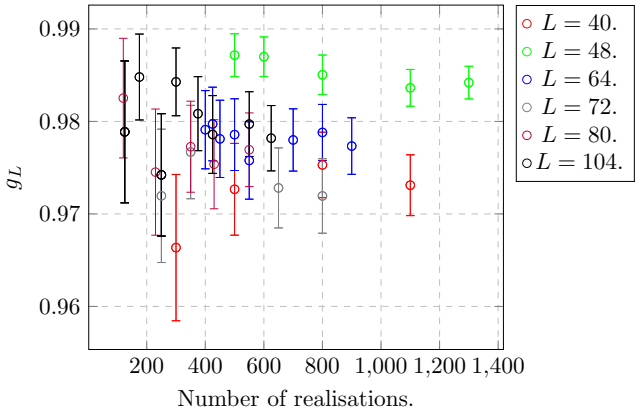

FIGURE 3.3: The uncertainty in the Binder cumulant as a function of the number of realisations at a point closest to $t/L^2 \log t$ for $t = 937.5$ (three quarters through the simualtion) for $L = 40$. $\lambda_x = \lambda_y 0$. There is no value for 128.

a function of $\log(t/\log t)$, shown in **??** to**??** for each system size. For the linear case, it is expected that $\log n_v = -\log(t/\log t)$. This can be explained as follows: using the result in [1] that the distance between vortices R is approximately proportional to $(t/\log t)^{1/2}$, we have that the vortex density is then $1/R^2$, and the number of vortices $n_v \sim L^2/R^2$, and therefore $\log n_v \sim -\log R^2 = -\log(t/\log t)$ up to some additive constants. For brevity, we shall call this the 'vortex gradient.' As the figures show, the gradient was obtained to good accuracy for all system sizes: taking an average for all sizes, we obtain the value -1.001 ± 0.003. Due to the finite size of the system, the approximation breaks down at large times once the majority of the vortices have annihilated, and therefore a time scale must be chosen with which to calculate the gradient. In practice, the time scale maximised but chosen to be prior to the finite size behaviour of the system. Therefore it is sensible not to read the values too literally, but take them as indicative of the behaviour of the linear case.

3.2 Anistropic Case

For non-zero λs, when $\lambda_x = -\lambda_y$, we expect to obtain the same result as the linear case. Figures **??** to **??** show the Binder cumulant plotted as a function of t and also $t/L^2 \log t$ for several values of increasing λ_x. Although the collapse is not as tight as for the linear case, it clearly still occurs to an extent, confirming the expectation. For the case $\lambda_x = 0.2$, the curves do not cross each other as closely as in the linear case at the mid-point of the simulation, however looking at the uncertainties shows that only the $L = 80$ size deviates from the others. All other points are within each other when considering the uncertainties. These conclusions also apply after three quarters of the simulation has completed. This is corroborated by the grandient in vortex gradient which is averaged to be -1.001 ± 0.003, demonstarted linear behaviour.

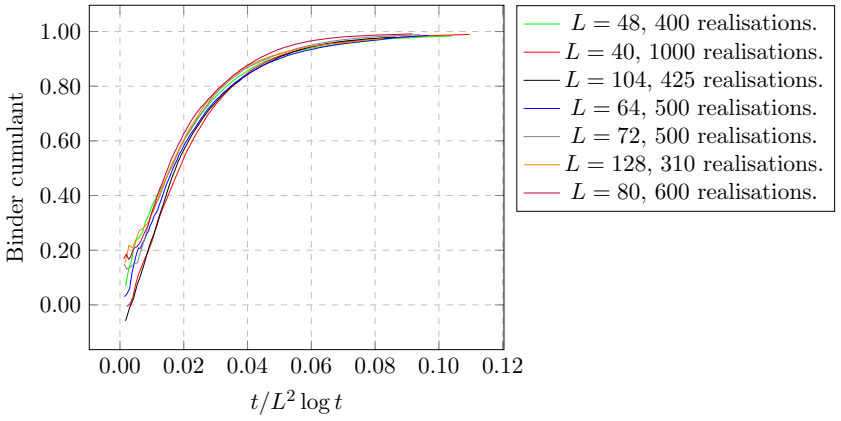

FIGURE 3.4: The Binder cumulant as a function of $t/L^2 \log t$ for different sizes with $\lambda_x = -\lambda_y = 0.2$.

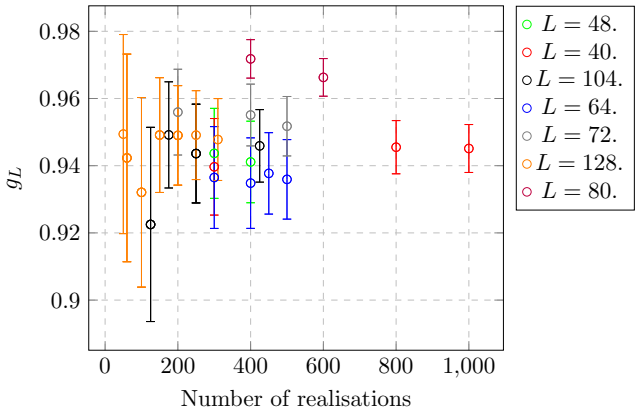

FIGURE 3.5: The uncertainty in the Binder cumulant as a function of the number of realisations at a point closest to $t/L^2 \log t$ for $t = 6500$ (the mid-point of the simulation) for $L = 40.\lambda_x = -\lambda_y = 0.2$.

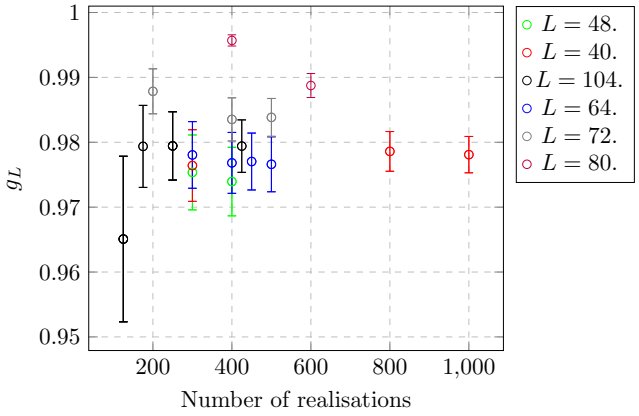

FIGURE 3.6: The uncertainty in the Binder cumulant as a function of the number of realisations at a point closest to $t/L^2 \log t$ for $t = 937.5$ (three quarters through the simualtion) for $L = 40$. $\lambda_x = -\lambda_y = 0.2$. There is no value for 128.

For $\lambda_x = 0.4$ there are similar conclusions to be made. $L = 80$ also deviates, while the mid point uncertainties in the Binder cumulant are within each other for other system sizes. Due to these errors on the Binder cumulant, it would appear that it is undetermined whether further realisations are necessary to tighten the collapse further, or if the dynamical exponent growth rate $(t/\log t)^{1/2}$ is simply not as good an approximation as in the linear case. On the other hand, the vortex gradient does show deviation in its calculated average of -1.013 ± 0.003. As these decrease for higher values of λ monotonically it is clear that the effects of higher values of λ are beginning to be felt. In particular, the convergence of the Binder cumulant becomes faster as λ increases, indicating a faster transition to the ordered phase.

To test how this effects the collapse of the Binder cumulant, we can reverse the process which determined the gradient from the correlation length. Therefore the Binder cumulant should be plotted as a function of $(t/logt)^{\alpha/2}$ where α is the gradient of the vortex plot. Similarly to how [1] plotted the collapse with an effective exponent $z = 2.35$, the

purpose of this plot does not have a physical origin but to demonstrate that the $t/\log t$ must be modified. It should be again noted that [**PhysRevB.94.104520**] only has calculations for the first and second order (in λ) terms for the force between vortices in the weakly isotropic case, where the terms were repulsive at large distances. In the following they appear to be attractive.

For $\lambda_x = 0.4$, the plot of the Binder cumulant as a function of $(t/\log t)^1.013/L^2$ is shown in XX. The collapse is only slightly tighter. The gradient, however, has not significantly deviated from the linear case, so this is not unexpected. In both cases the collapse is still weaker than the linear case. Noting the previous comments on the uncertainties, further simulations are indeed necessary, but there are also are differences to the linear case.

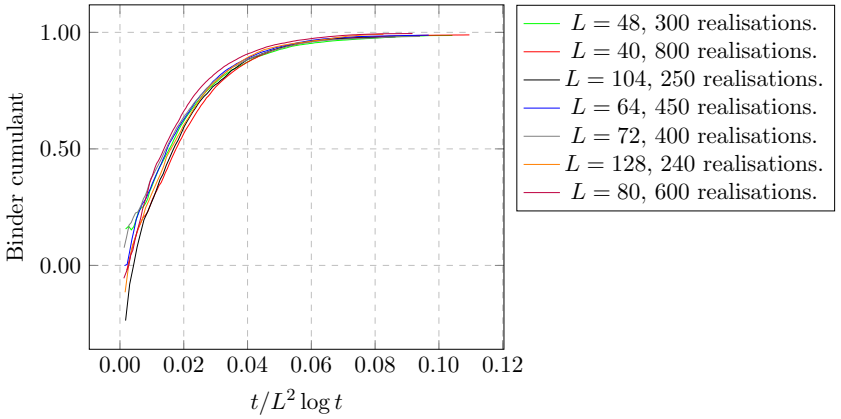

FIGURE 3.7: The Binder cumulant as a function of $t/L^2 \log t$ for different sizes with $\lambda_x = -\lambda_y = 0.4$.

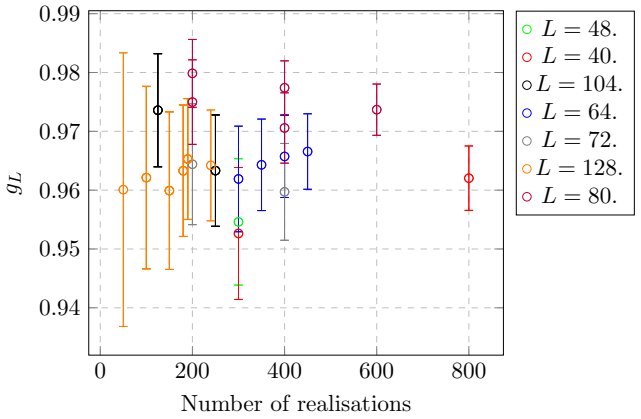

FIGURE 3.8: The uncertainty in the Binder cumulant as a function of the number of realisations at a point closest to $t/L^2 \log t$ for $t = 6500$ (the mid-point of the simulation) for $L = 40.\lambda_x = -\lambda_y = 0.4$.

For the remaining values of λ, we compare both the collapse with an exponent $\alpha = 1$ and one calculated from the gradient. As one increases λ the collapse becomes weaker with a linear exponent but does not appear to degrade in any linear fashion with the

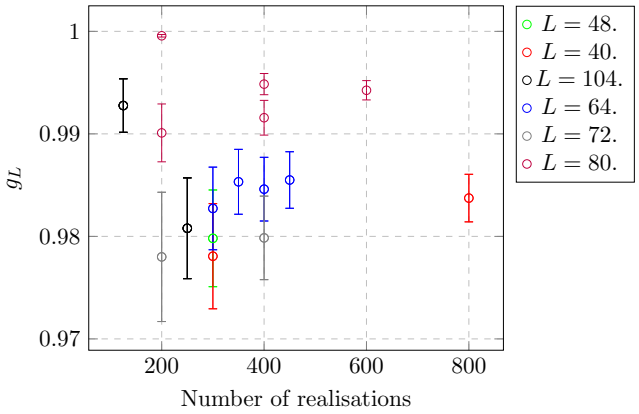

FIGURE 3.9: The uncertainty in the Binder cumulant as a function of the number of realisations at a point closest to $t/L^2 \log t$ for $t = 937.5$ (three quarters through the simualtion) for $L = 40$. $\lambda_x = \lambda_y - 0.4$ There is no value for 128.

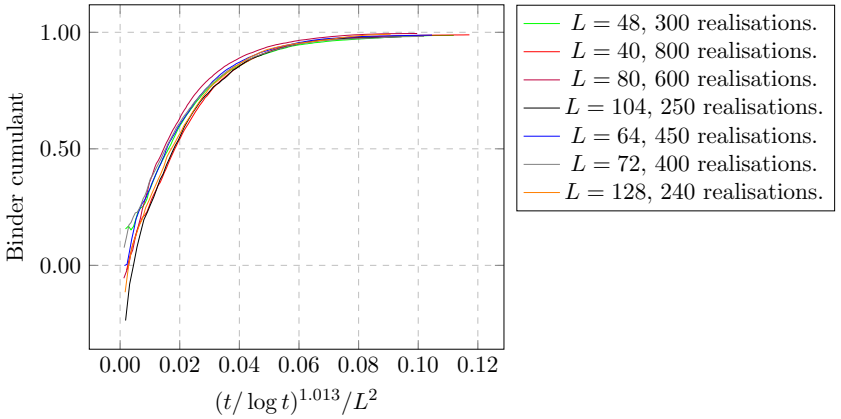

FIGURE 3.10: The Binder cumulant as a function of $(t/\log t)^{1.013}/L^2$ for different sizes with $\lambda_x = -\lambda_y = 0.4$.

modified exponent. In fact, a subjective glance seems to indicate it actually improves, with $\lambda = 1.5$ showing the strongest collapse besides the linear case.

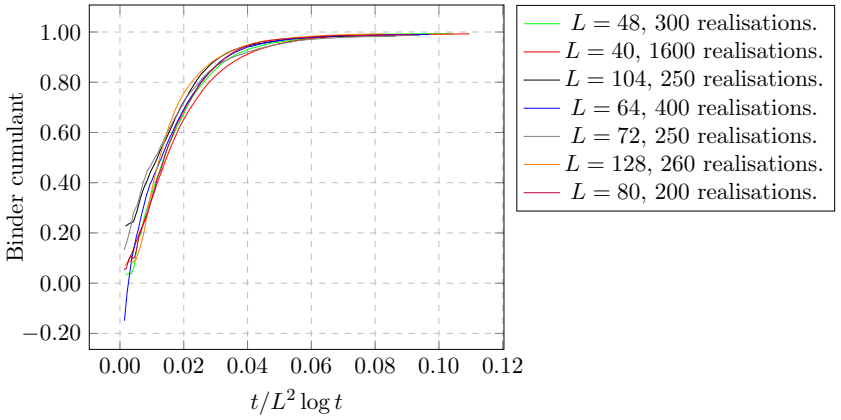

FIGURE 3.11: The Binder cumulant as a function of $t/L^2 \log t$ for different sizes with $\lambda_x = -\lambda_y = 0.6$.

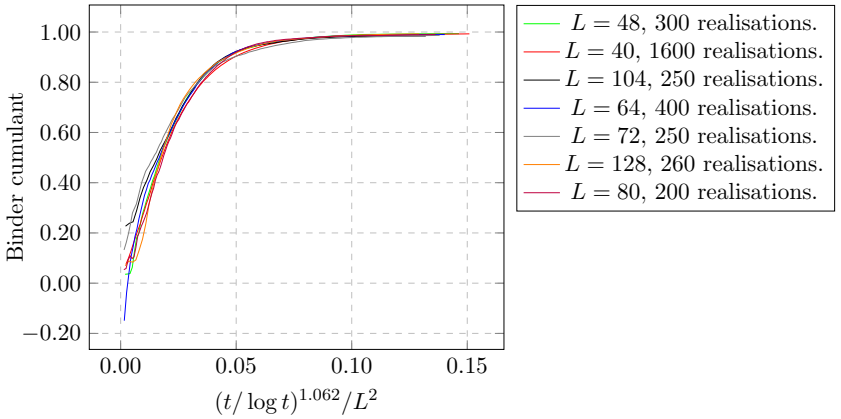

FIGURE 3.12: The Binder cumulant as a function of $(t/\log t)^{1.062}/L^2$ for different sizes with $\lambda_x = -\lambda_y = 0.6$.

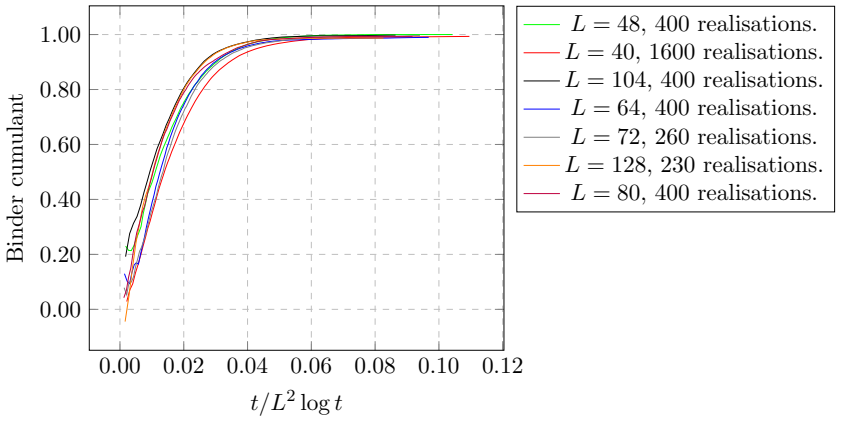

FIGURE 3.13: The Binder cumulant as a function of $t/L^2 \log t$ for different sizes with $\lambda_x = -\lambda_y = 0.8$.

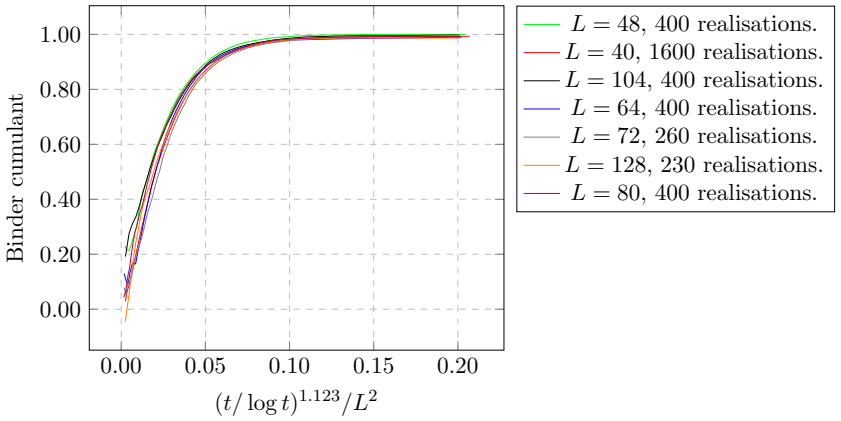

FIGURE 3.14: The Binder cumulant as a function of $(t/\log t)^{1.123}/L^2$ for different sizes with $\lambda_x = -\lambda_y = 0.8$.

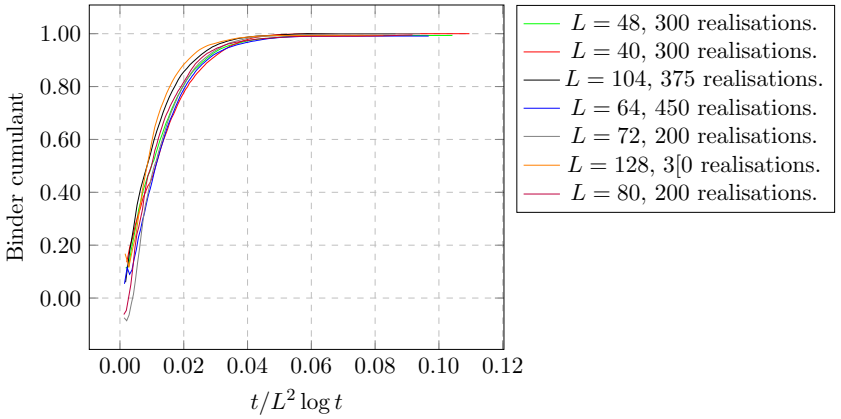

FIGURE 3.15: The Binder cumulant as a function of $t/L^2 \log t$ for different sizes with $\lambda_x = -\lambda_y = 1$.

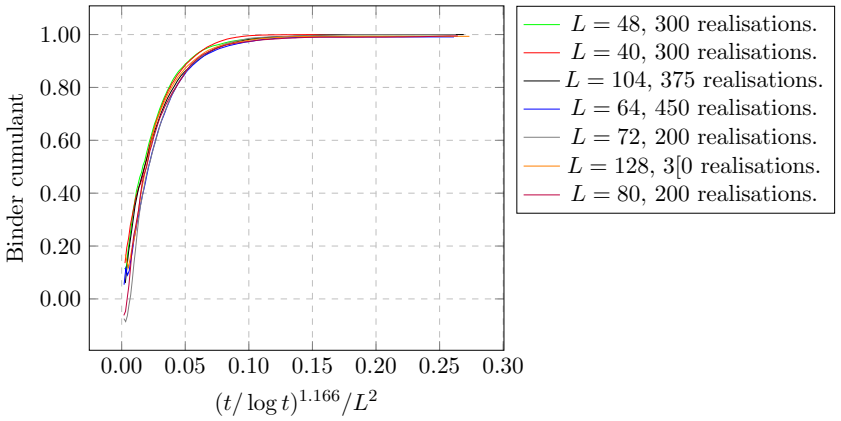

FIGURE 3.16: The Binder cumulant as a function of $(t/\log t)^{1.166}/L^2$ for different sizes with $\lambda_x = -\lambda_y = 1$.

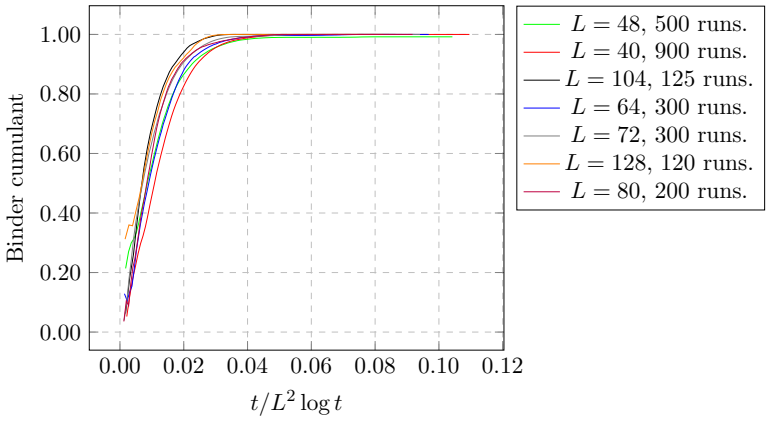

FIGURE 3.17: The Binder cumulant as a function of $t/L^2 \log t$ for different sizes with $\lambda_x = -\lambda_y = 1.5$.

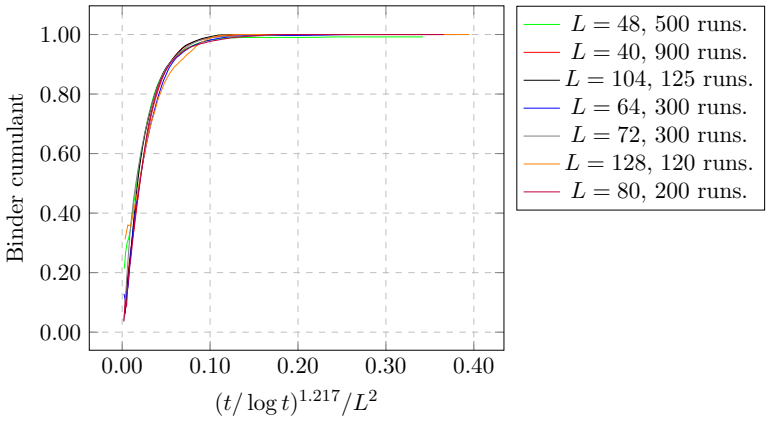

FIGURE 3.18: The Binder cumulant as a function of $(t/\log t)^{1.217}$ for different sizes with $\lambda_x = -\lambda_y = 1.5$.

To check if this is perhaps a finite size effect, although there is no immediate indication that this should be the case, with the calculations in [**PhysRevX.7.041006**] showing that spatial correlations are algebraic as in the XY model below the BKT transitions, the gradient was check for system sizes of $L = 512$. This was for $\mathrm{d}t = 0.05$ and a much lower number of realisations, so not directly comparable, but at least the behaviour of decreasing gradient with increasing λ also follows. Further study into these areas is clearly necessary.

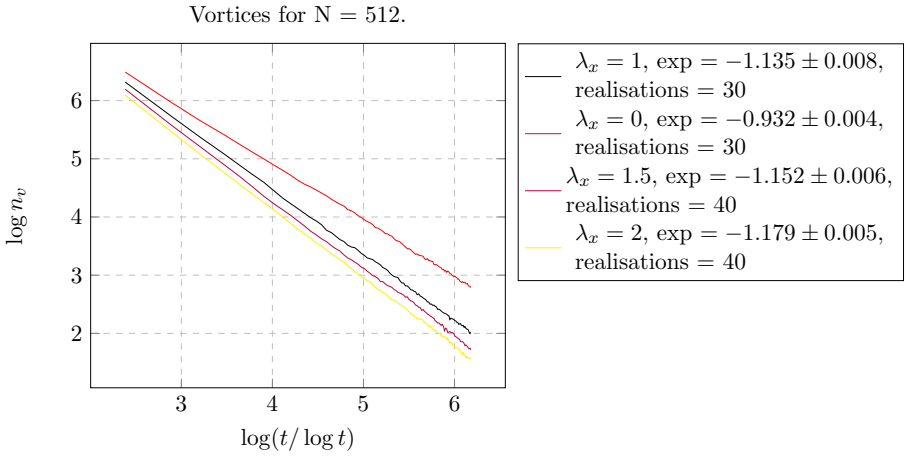

FIGURE 3.19: Log of the number of vortices as a function of $\log(t/\log t)$ for $L = 512$ in the anistropic case.

3.3 Isotrpic case

In the isotropic case, due to the non-linearity, we expect a repulsive contribution of the vortex force at large calculated in [**PhysRevB.94.104520**] with the second order

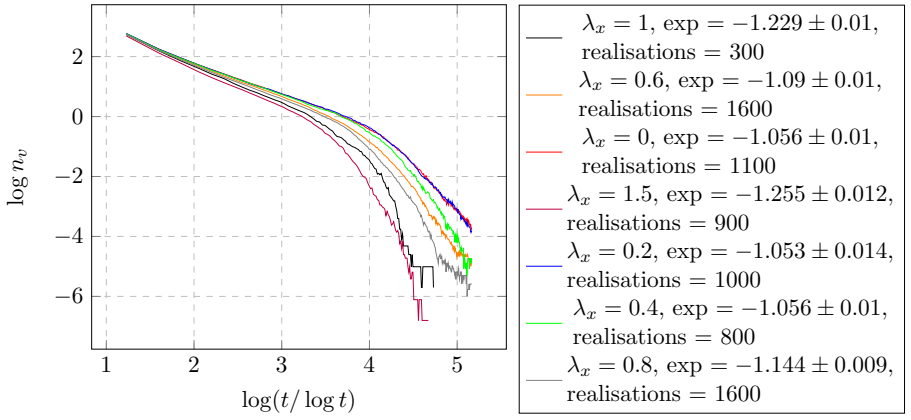

FIGURE 3.20: Log of the number of vortices as a function of $\log(t/\log t)$ for $L = 40$ in the anistropic case.

??

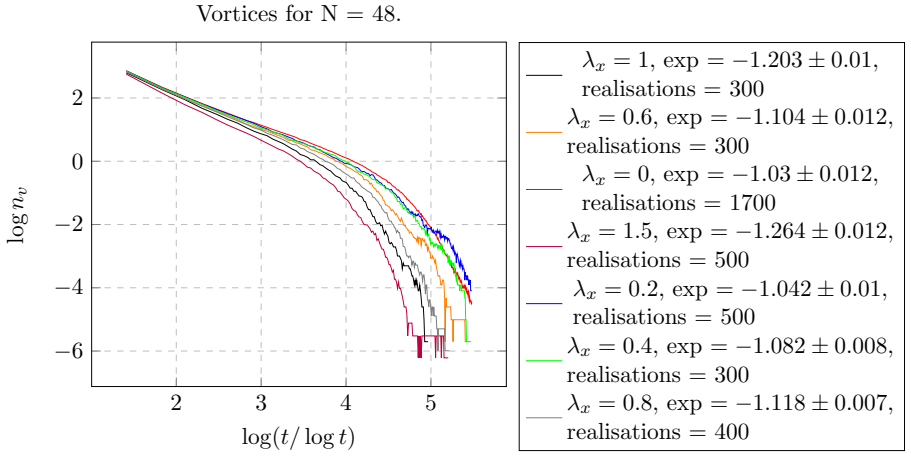

FIGURE 3.21: Log of the number of vortices as a function of $\log(t/\log t)$ for $L = 48$ in the anistropic case.

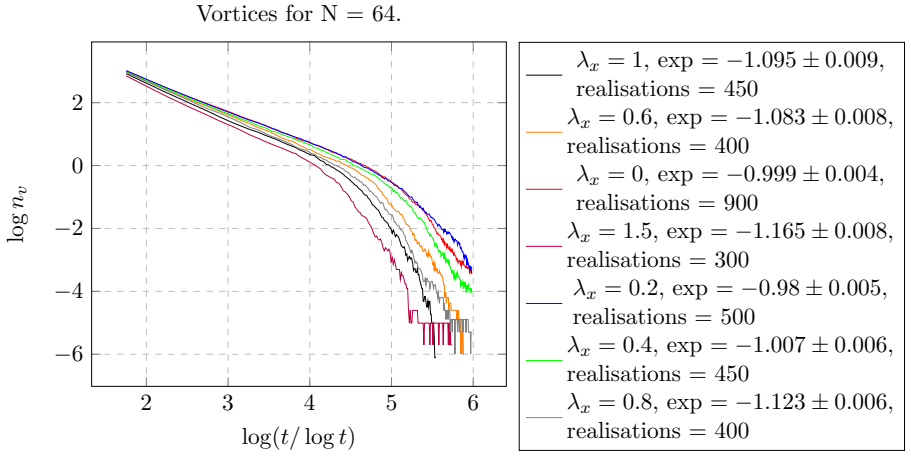

FIGURE 3.22: Log of the number of vortices as a function of $\log(t/\log t)$ for $L = 64$ in the anistropic case.

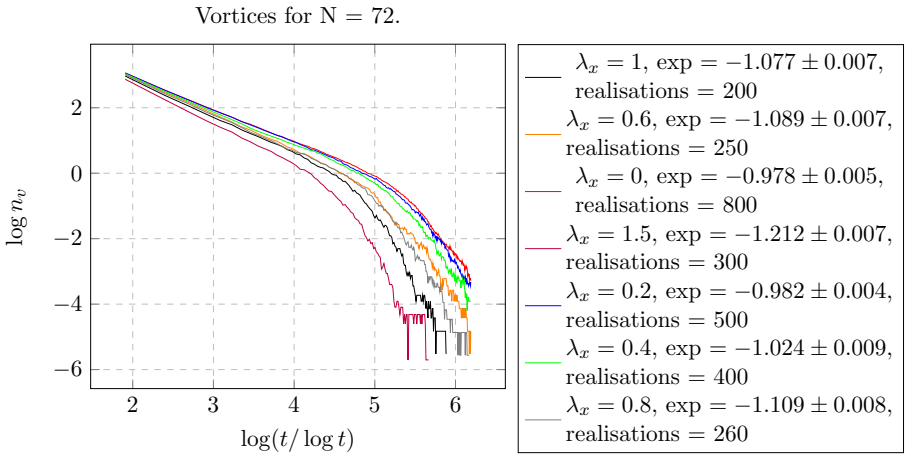

FIGURE 3.23: Log of the number of vortices as a function of $\log(t/\log t)$ for $L = 72$ in the anistropic case.

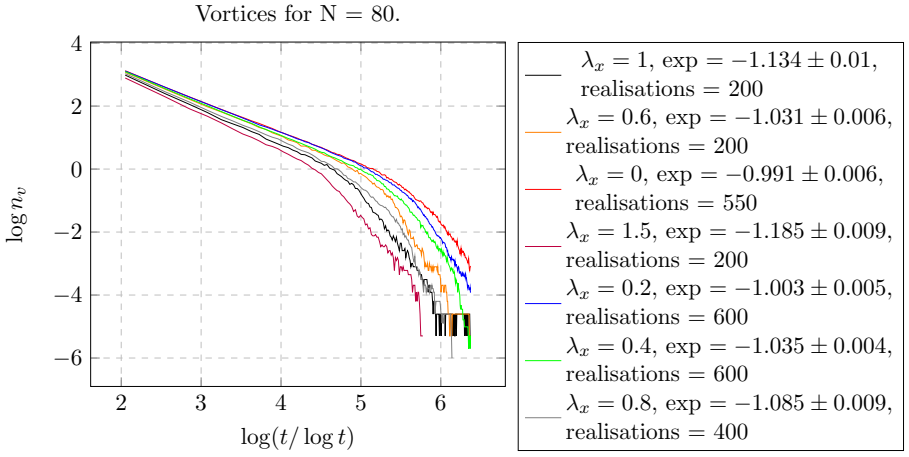

FIGURE 3.24: Log of the number of vortices as a function of $\log(t/\log t)$ for $L = 80$ in the anistropic case.

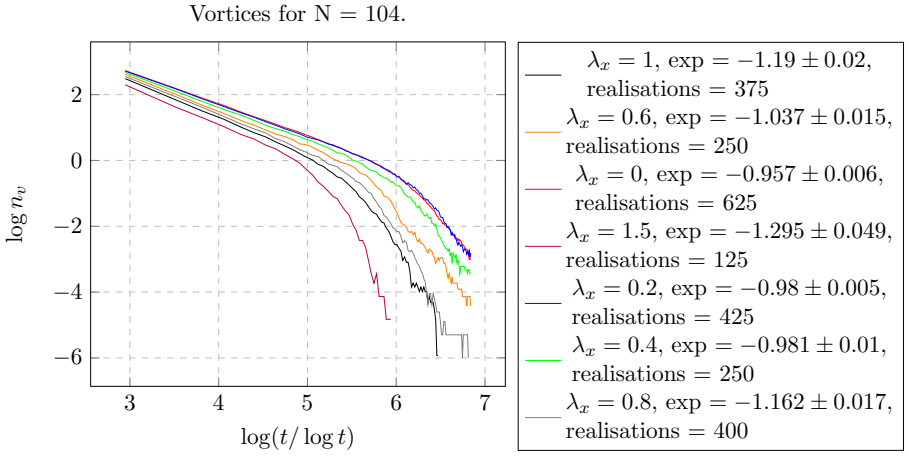

FIGURE 3.25: Log of the number of vortices as a function of $\log(t/\log t)$ for $L = 104$ in the anistropic case.

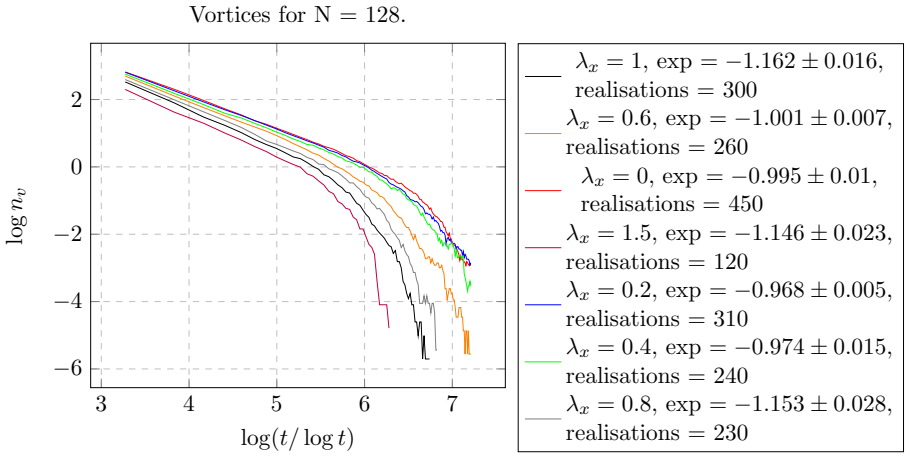

FIGURE 3.26: Log of the number of vortices as a function of $\log(t/\log t)$ for $L = 128$ in the anistropic case.

result, the first order being a force perpendicular to the line joining the vortices, of

$$\boldsymbol{f}(\boldsymbol{R}) = \frac{1}{8}\left(\frac{\lambda}{2D}\right)^2 + \frac{1}{\epsilon}\frac{\boldsymbol{R}}{R^2}(8\log(R/a)^2 + 4\log(R/a) - 1)$$

where R is the vortex separation, ϵ the dielectric constant, and a the lattice spacing. Thus, beyond a certain length scale vortex unbinding should occur–the vortex dominated phase–although this is not the same as the entropic unbinding in the XY case, estimated from equlibrium thermodynamics. Also in the paper the estimate for distance at which this correction term dominates and is given by

$$L_v = ae^{\frac{2D}{\lambda}}.$$

These conclusions are matched by the results. Figure. **??** shows the collapse for $\lambda_x = 0.2$ and the quality is comparable to the anisotropic case. This is as anticipated as we do not expect drastic change in the qualitative behaviour away from a critical point, and provides further confidence in the obtained results. Although the points in the uncertainty graph appear to all cross each other when including the errors, the uncertainties are much larger. The average vortex gradient is -0.953 ± 0.005, so has already altered unlike in the anisotropic case. This is in the direction we expect, where the the vortex recombination occurs at a slower rate due to their reduced attractions. In brief, the behaviour is slighty but not significantly different from the linear case.

Figures XX and XX show the uncertainties for $\lambda_x = 0.2$.

The case $\lambda_x = 0.4$ is more interesting, where the efefcts of the non-linearity are much more pronounced. This provides a clear demonstration of the expectation in that the 'destruction' of the convergence of the Binder cumulant occurs first for the largest system

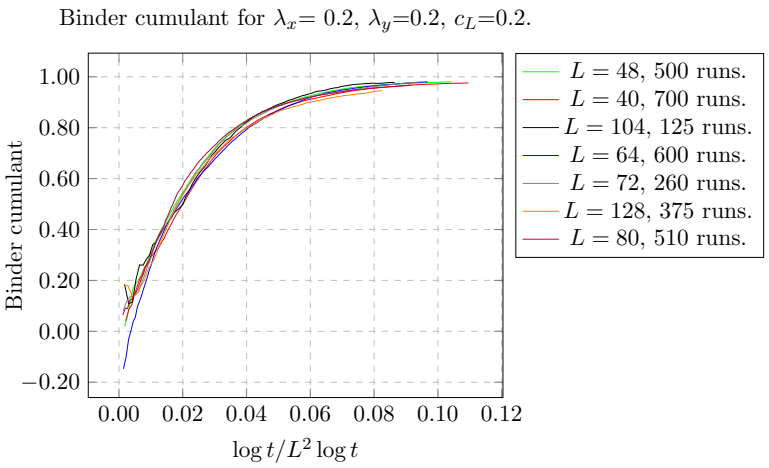

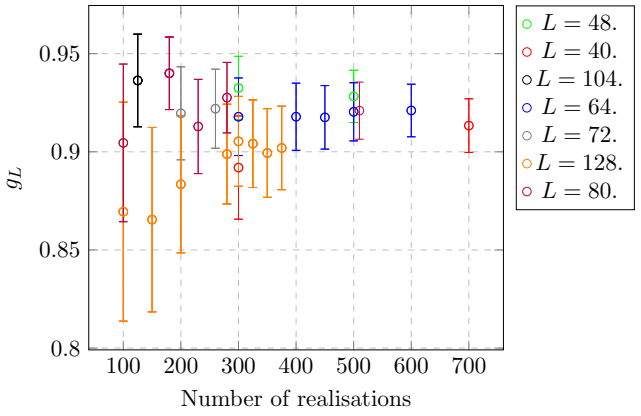

FIGURE 3.27: The uncertainty in the Binder cumulant as a function of the number of realisations at a point closest to $t/L^2 \log t$ for $t = 6500$ (the mid-point of the simulation) for $L = 40.\lambda_x = \lambda_y = 0.2$.

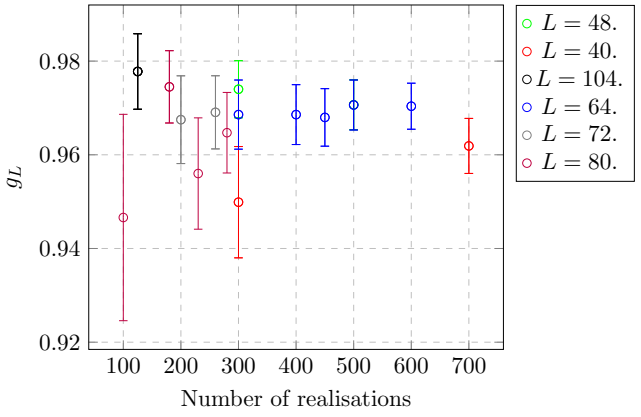

FIGURE 3.28: The uncertainty in the Binder cumulant as a function of the number of realisations at a point closest to $t/L^2 \log t$ for $t = 9370$ (the mid-point of the simulation) for $L = 40.\lambda_x = \lambda_y = 0.2$.

and gradually lessens for the smaller system as can be seen from the order of the curves in the plot. There is also a weak pattern in the increase of the vortex gradient as the system size is increased, ranging from -0.928 ± 0.015 for $L = 40$ to -0.807 ± 0.009 for $L = 128$, whereas no such pattern occurs in the linear case.

As for the uncertainties, they are all larger and in general the points are not overlapping, although this can be seen from the graph of the Binder cumulant. The uncertainty in the sizes $L = 104$ and $L = 128$ are much larger, and the for these sizes the Binder cumulant is fluctuating.

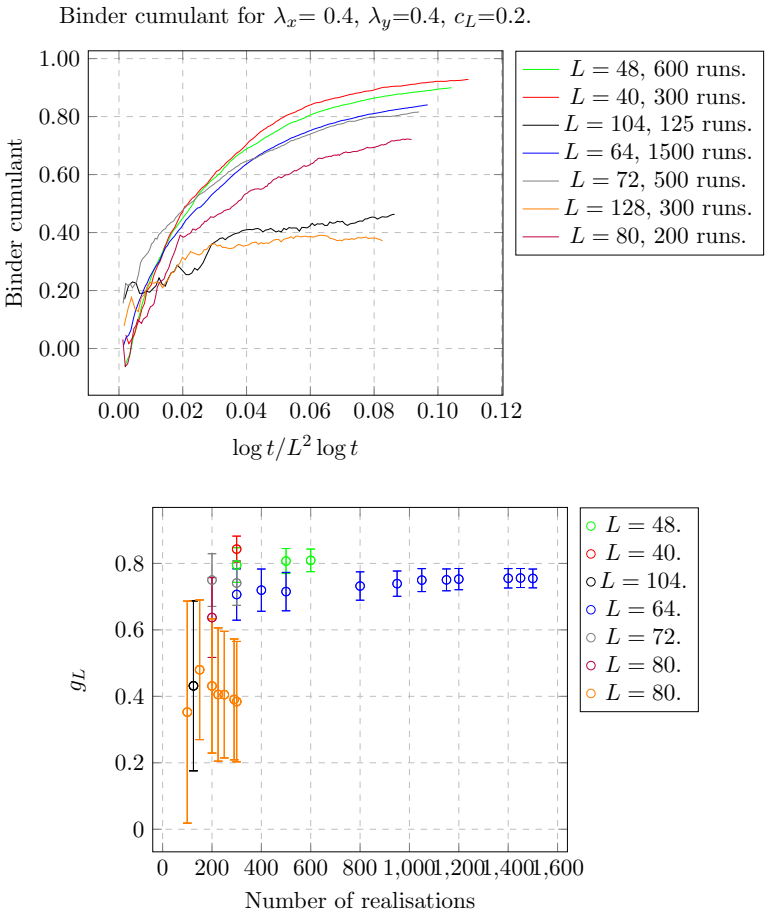

FIGURE 3.29: The uncertainty in the Binder cumulant as a function of the number of realisations at a point closest to $t/L^2 \log t$ for $t = 650$ (three quarters through the simualtion) for $L = 40$. $\lambda_x = \lambda_y = 0.4$.

By observing the behaviour of the Binder cumulant as λ is increased further, a clear pattern emerges. The largest systems ($L = 128$ and $L = 104$) first fluctuate around 0 with a negative bias before fluctuating with an amplitude of around 0.5. Smaller systems, in order, first begin decreasing significantly and also fluctuating quite severely, which explains the very large uncertainties (not shown) obtained, before finally also fluctuating around 0 with the same amplitude. For the larger systems this occurs at $\lambda_x = 0.6$ to $\lambda_x = 0.8$, while $L = 72$ and $L = 80$ are finally fluctuating around 0 by $\lambda_x = 1$.

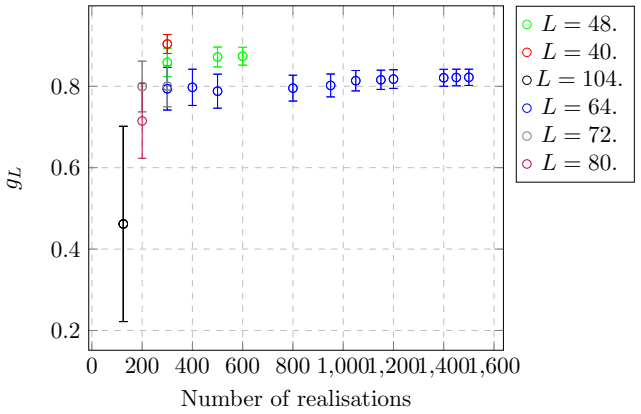

FIGURE 3.30: The uncertainty in the Binder cumulant as a function of the number of realisations at a point closest to $t/L^2 \log t$ for $t = 937.5$ (three quarters through the simualtion) for $L = 40$. $\lambda_x = \lambda_y = 0.4$. There is no value for 128.

The plots do not show the very large negative values obtained by the systems, which increases on a system size decrease. This can potentially be explained as the Binder cumulant is a ratio of two quantities in the disordered state, so may be very large. We do not show the plots for $\langle \boldsymbol{M}^2 \rangle$: it suffices to point out that the value is close to zero. While for a completely random phase angle at each point the Binder cumulant should be zero, this may not be the case in this regime. This transition stabilises eventually. The larger decrease during the transition for small sizes could be due to the structure of the vortex interactions or also the lower number of phase points used in calculating the magnetisation. In this way, the behaviour may be a finite size effect: both the speed of the transition to the fluctuation about 0 and the severity of the behaviour of the Binder cumulant was reduced for larger system sizes.

For the gradient of the vortices, it behaves as expected for smaller values of λ in that increasing λ results in the gradient increasing. The repulsive force due to the non linearity should either prevent the vortices from recombining, or slow their rate of recombination. The upshot means that for high enough values of λ there should be a saturation on the number of vortices, at least on large enough systems. The caveat of a large system is because initially the vortex density is very higher which means that vortices closest to each other can recombine and only after the vortex density is low enough does the saturation take place. In previous simulations that have been performed, eventually the number of vortices saturates for system sizes of $L = 512$.

The slightly concerning nature of these graphs is that at a sufficiently large λ the gradient actually *decreases* again, and this occurs for all system sizes with the rate being faster the larger the system. To ensure this is not perhaps a finite size effect or a numerical artefact, a simulation with size $L = 512$ was performed as shown in XX. Here a saturation is obtained, matching the previous result. However, the decrease in the gradient also

occurs around the same values of λ as in the other system sizes, so further investigation is required.

Binder cumulant for λ_x= 0.6, λ_y=0.6, c_L=0.2.

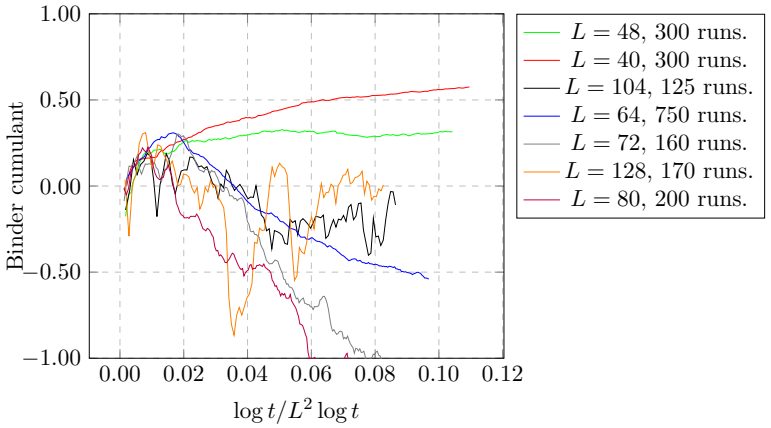

Binder cumulant for λ_x= 0.8, λ_y=0.8, c_L=0.2.

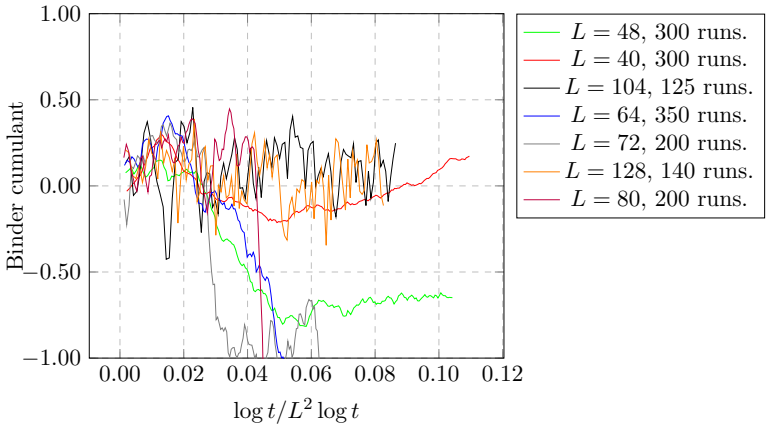

Binder cumulant for λ_x= 1, λ_y=1, c_L=0.2.

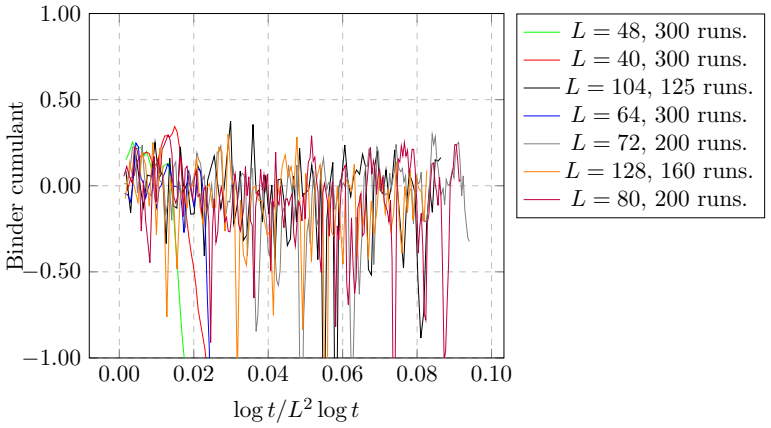

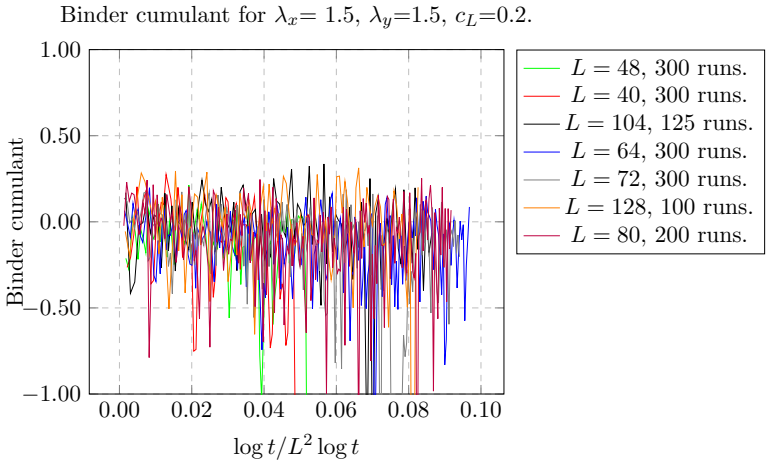
Binder cumulant for λ_x= 1.5, λ_y=1.5, c_L=0.2.
Binder cumulant
1.00
0.50
0.00
−0.50
−1.00
0.00
0.02
0.04
0.06
0.08
0.10
$\log t/L^2 \log t$
$L = 48$, 300 runs.
$L = 40$, 300 runs.
$L = 104$, 125 runs.
$L = 64$, 300 runs.
$L = 72$, 300 runs.
$L = 128$, 100 runs.
$L = 80$, 200 runs.

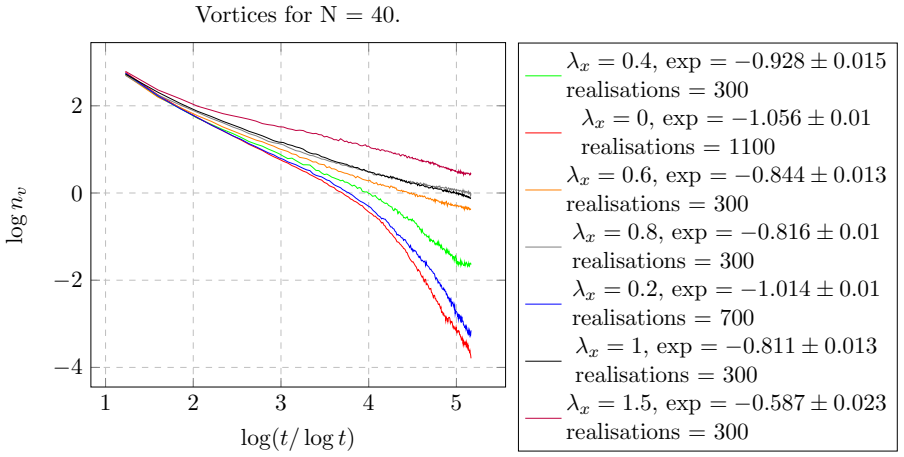
Vortices for N = 40.
$\log n_v$
2
0
−2
−4
1
2
3
4
5
$\log(t/\log t)$
$\lambda_x = 0.4$, exp = -0.928 ± 0.015
realisations = 300
$\lambda_x = 0$, exp = -1.056 ± 0.01
realisations = 1100
$\lambda_x = 0.6$, exp = -0.844 ± 0.013
realisations = 300
$\lambda_x = 0.8$, exp = -0.816 ± 0.01
realisations = 300
$\lambda_x = 0.2$, exp = -1.014 ± 0.01
realisations = 700
$\lambda_x = 1$, exp = -0.811 ± 0.013
realisations = 300
$\lambda_x = 1.5$, exp = -0.587 ± 0.023
realisations = 300

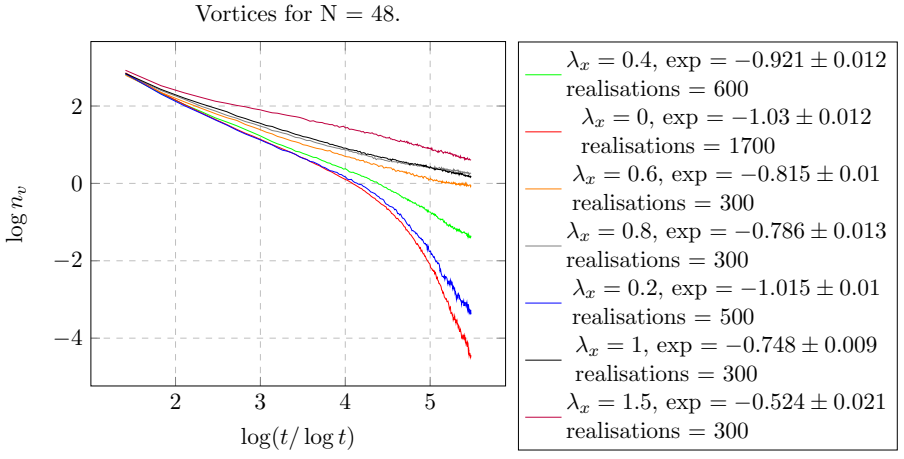
Vortices for N = 48.
$\log n_v$
2
0
−2
−4
2
3
4
5
$\log(t/\log t)$
$\lambda_x = 0.4$, exp = -0.921 ± 0.012
realisations = 600
$\lambda_x = 0$, exp = -1.03 ± 0.012
realisations = 1700
$\lambda_x = 0.6$, exp = -0.815 ± 0.01
realisations = 300
$\lambda_x = 0.8$, exp = -0.786 ± 0.013
realisations = 300
$\lambda_x = 0.2$, exp = -1.015 ± 0.01
realisations = 500
$\lambda_x = 1$, exp = -0.748 ± 0.009
realisations = 300
$\lambda_x = 1.5$, exp = -0.524 ± 0.021
realisations = 300

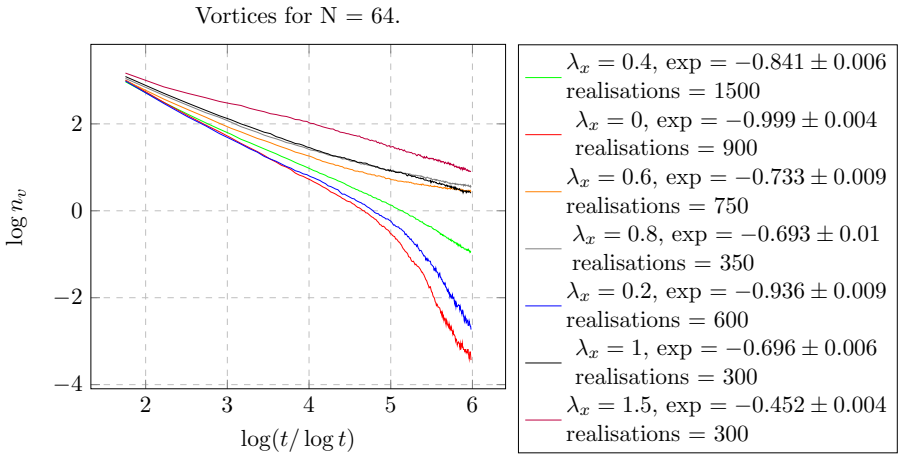
Vortices for N = 64.
log n_v
log(t/ log t)
$\lambda_x = 0.4$, exp = -0.841 ± 0.006 realisations = 1500
$\lambda_x = 0$, exp = -0.999 ± 0.004 realisations = 900
$\lambda_x = 0.6$, exp = -0.733 ± 0.009 realisations = 750
$\lambda_x = 0.8$, exp = -0.693 ± 0.01 realisations = 350
$\lambda_x = 0.2$, exp = -0.936 ± 0.009 realisations = 600
$\lambda_x = 1$, exp = -0.696 ± 0.006 realisations = 300
$\lambda_x = 1.5$, exp = -0.452 ± 0.004 realisations = 300

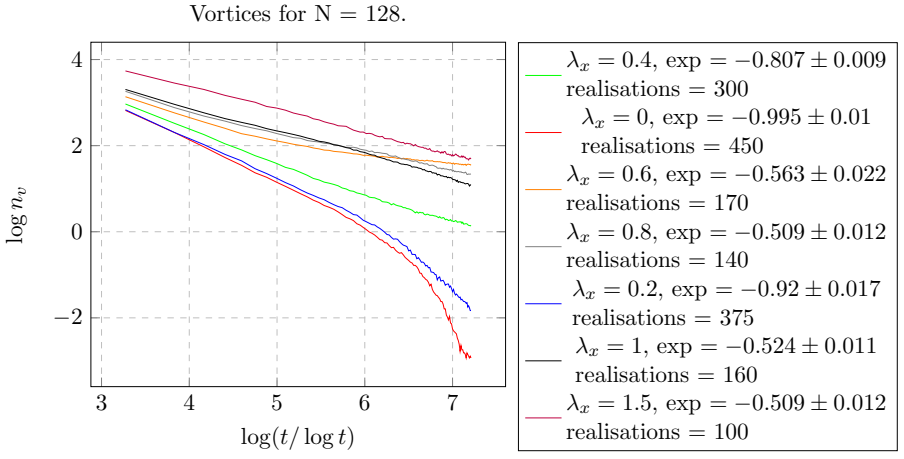
Vortices for N = 128.
log n_v
log(t/ log t)
$\lambda_x = 0.4$, exp = -0.807 ± 0.009 realisations = 300
$\lambda_x = 0$, exp = -0.995 ± 0.01 realisations = 450
$\lambda_x = 0.6$, exp = -0.563 ± 0.022 realisations = 170
$\lambda_x = 0.8$, exp = -0.509 ± 0.012 realisations = 140
$\lambda_x = 0.2$, exp = -0.92 ± 0.017 realisations = 375
$\lambda_x = 1$, exp = -0.524 ± 0.011 realisations = 160
$\lambda_x = 1.5$, exp = -0.509 ± 0.012 realisations = 100

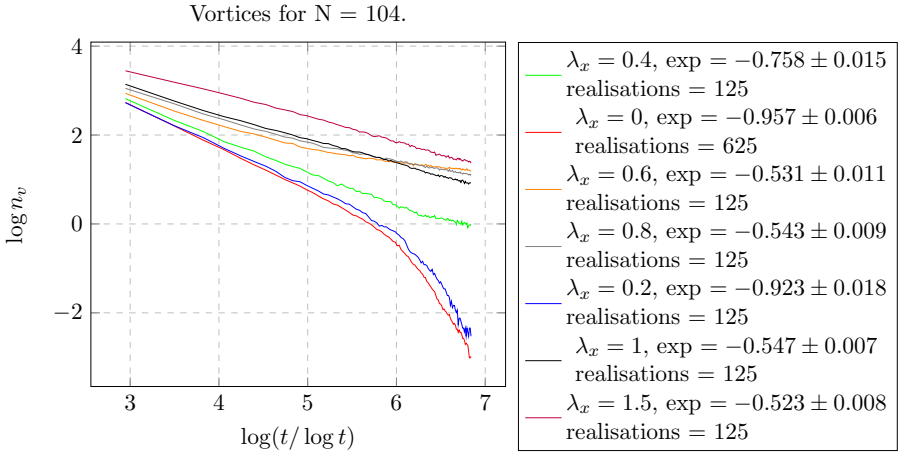
Vortices for N = 104.
log n_v
log(t/ log t)
$\lambda_x = 0.4$, exp = -0.758 ± 0.015 realisations = 125
$\lambda_x = 0$, exp = -0.957 ± 0.006 realisations = 625
$\lambda_x = 0.6$, exp = -0.531 ± 0.011 realisations = 125
$\lambda_x = 0.8$, exp = -0.543 ± 0.009 realisations = 125
$\lambda_x = 0.2$, exp = -0.923 ± 0.018 realisations = 125
$\lambda_x = 1$, exp = -0.547 ± 0.007 realisations = 125
$\lambda_x = 1.5$, exp = -0.523 ± 0.008 realisations = 125

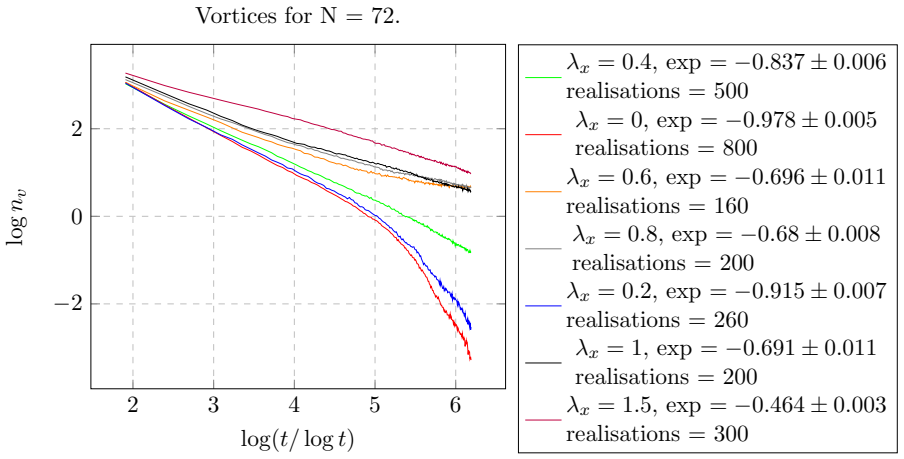
Vortices for N = 72.
log n_v
2
0
−2
2
3
4
5
6
log(t/ log t)
$\lambda_x = 0.4$, exp $= -0.837 \pm 0.006$
realisations $= 500$
$\lambda_x = 0$, exp $= -0.978 \pm 0.005$
realisations $= 800$
$\lambda_x = 0.6$, exp $= -0.696 \pm 0.011$
realisations $= 160$
$\lambda_x = 0.8$, exp $= -0.68 \pm 0.008$
realisations $= 200$
$\lambda_x = 0.2$, exp $= -0.915 \pm 0.007$
realisations $= 260$
$\lambda_x = 1$, exp $= -0.691 \pm 0.011$
realisations $= 200$
$\lambda_x = 1.5$, exp $= -0.464 \pm 0.003$
realisations $= 300$

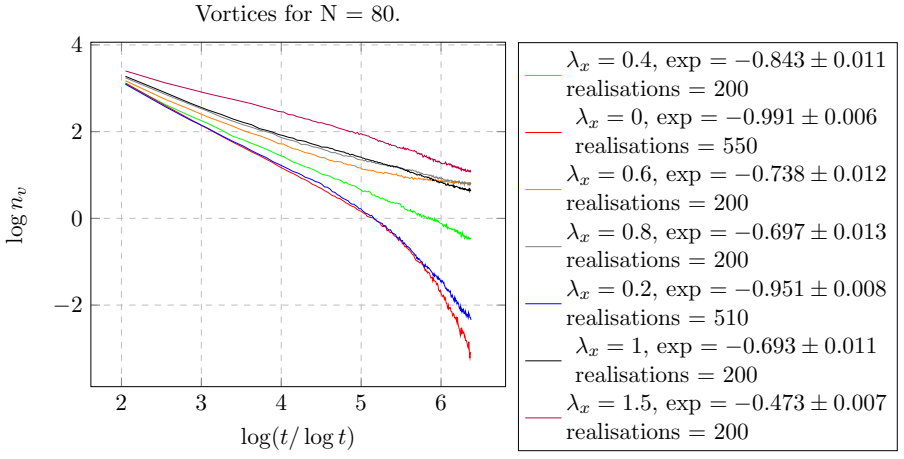
Vortices for N = 80.
log n_v
4
2
0
−2
2
3
4
5
6
log(t/ log t)
$\lambda_x = 0.4$, exp $= -0.843 \pm 0.011$
realisations $= 200$
$\lambda_x = 0$, exp $= -0.991 \pm 0.006$
realisations $= 550$
$\lambda_x = 0.6$, exp $= -0.738 \pm 0.012$
realisations $= 200$
$\lambda_x = 0.8$, exp $= -0.697 \pm 0.013$
realisations $= 200$
$\lambda_x = 0.2$, exp $= -0.951 \pm 0.008$
realisations $= 510$
$\lambda_x = 1$, exp $= -0.693 \pm 0.011$
realisations $= 200$
$\lambda_x = 1.5$, exp $= -0.473 \pm 0.007$
realisations $= 200$

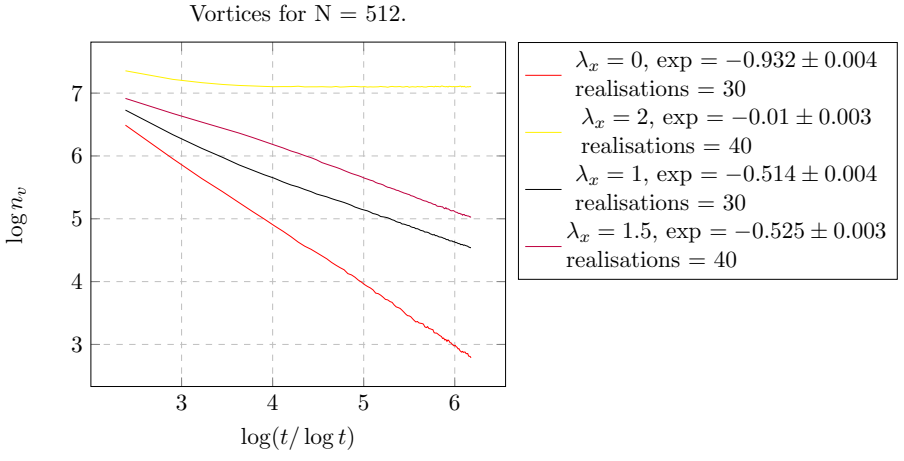
Vortices for N = 512.
log n_v
7
6
5
4
3
3
4
5
6
log(t/ log t)
$\lambda_x = 0$, exp $= -0.932 \pm 0.004$
realisations $= 30$
$\lambda_x = 2$, exp $= -0.01 \pm 0.003$
realisations $= 40$
$\lambda_x = 1$, exp $= -0.514 \pm 0.004$
realisations $= 30$
$\lambda_x = 1.5$, exp $= -0.525 \pm 0.003$
realisations $= 40$